U(VI) Reduction by Biogenic and Abiotic Hydroxycarbonate Green Rusts: Impacts on U(IV) Speciation and Stability Over Time

Sen Yan,[1,2*] Maxim I. Boyanov,[2,3] Bhoopesh Mishra,[2,4] Kenneth M. Kemner,[2] and
Edward J. O'Loughlin[2*]

1. School of Earth Sciences, China University of Geosciences, Wuhan, 430074, China
(sen.yan@cug.edu.cn)
2. Biosciences Division, Argonne National Laboratory, Argonne, IL, 60439, USA
(oloughlin@anl.gov, kemner@anl.gov)
3. Institute of Chemical Engineering, Bulgarian Academy of Sciences, Sofia, 1113, Bulgaria
(mboyanov@ice.bas.bg)
4. School of Chemical and Process Engineering, University of Leeds, Leeds, LS2 9JT, UK
(b.mishra@leeds.ac.uk)

---

[*] Corresponding author (SY) phone: (86) 27-67883033; fax: (86) 27-67883001; e-mail: sen.yan@cug.edu.cn; address: School of Earth Sciences, China University of Geosciences, 388 Lumo Road, Wuhan, China, 430074.

[*] Corresponding author (EJO) phone: (630) 252-9902; e-mail: oloughlin@anl.gov; address: Biosciences Division, Argonne National Laboratory, Building 203, Room E-137, 9700 South Cass Ave., Argonne, IL 60439-4843.

ABSTRACT

Green rusts (GRs) are redox active Fe^{II}-Fe^{III} minerals that form in the environment via various biotic and abiotic processes. Although both biogenic (BioGR) and abiotic (ChemGR) GRs have been shown to reduce U^{VI}, the dynamics of the transformations and the speciation and stability of the resulting U^{IV} phases are poorly understood. We used carbonate extraction and XAFS spectroscopy to investigate the products of U^{VI} reduction by BioGR and ChemGR. The results show that both GRs can rapidly remove U^{VI} from synthetic groundwater via reduction to U^{IV}. The initial products in the ChemGR system are solids-associated U^{IV}-carbonate complexes that gradually transform to nanocrystalline uraninite over time, leading to a decrease in the proportion of carbonate-extractable U from ~95% to ~10%. In contrast, solid-phase U^{IV} atoms in the BioGR system remain relatively extractable, non-uraninite U^{IV} species over the same reaction period. The presence of calcium and carbonate in groundwater significantly increase the extractability of U^{IV} in the BioGR system. These data provide new insights into the transformations of U under anoxic conditions in groundwater that contains calcium and carbonate, and have major implications for predicting uranium stability within redox dynamic environments and designing approaches for the remediation of uranium-contaminated groundwater.

INTRODUCTION

Uranium (U) is a contaminant at numerous uranium mining, ore processing, nuclear energy, and weapons-related sites. Indeed, nearly 70% of U.S. Department of Energy facilities report groundwater contamination by uranium.[1] The predominant valence states of uranium in groundwater are U^{VI} and U^{IV},[2] and the reduction of soluble uranyl ($U^{VI}O_2^{2+}$) to sparingly soluble U^{IV} forms such as uraninite and non-uraninite U^{IV} species has been explored as a basis for managing uranium mobility at contaminated sites. Past studies have indicated that mixtures of uraninite and non-uraninite U^{IV} species can form as products of U^{VI} reduction in reduced sediments.[3-5] Although some of the factors controlling the formation and stability of non-uraninite U^{IV} species have been determined,[6-8] much remains unknown concerning the effects of ligands and mineral surfaces on U^{IV} speciation and the stability and transformation of the U^{IV} products. Understanding the structure and transformation of these U^{IV} products is crucial for understanding their long-term stability and the processes controlling the fate and mobility of U in natural and engineered environments.

Green rusts (GRs) are mixed-valence Fe^{II}-Fe^{III} minerals found in redox transition zones in a variety of suboxic and anoxic environments including surface waters,[9] groundwater,[10, 11] soils,[12-14] and sediments.[15-17] GRs are redox active and may play a role in the fate and transformation of many organic[18, 19] and inorganic contaminants,[20-23] including uranium. GRs can form via various microbial and abiotic processes under circumneutral to alkaline conditions in suboxic environments.[24-31] Biogenic (BioGR) and abiotic (ChemGR) GRs have different surface properties, attributed largely to sorption of extracellular polymeric substances (EPSs) on BioGRs that passivate their surface, thereby inhibiting their reactivity toward contaminants such as nitrate and methyl red.[32, 33] However, Remy et al. found no significant difference in reactivity between BioGR and ChemGR with respect to the reduction of Hg^{II}.[33] In previous studies, we showed that both abiotic hydroxysulfate GR[34] and biogenic hydroxycarbonate GR[35] can rapidly remove U^{VI} from solution via reduction to U^{IV} in the form of uraninite nanoparticles in batch reactors containing deionized water. Moreover, Latta et al. found that U^{VI} was reduced to monomeric-type U^{IV} species by three different ChemGRs in deionized water containing TAPS buffer, and variable extents of U^{VI} reduction (34% to 100%) were observed for hydroxycarbonate GR with and without TAPS buffer.[36] The chemical speciation of U^{VI} can also have significant effects on its redox reactivity. For example, U^{VI} can form relatively stable and soluble complexes in the presence of calcium and carbonate, which are common constituents in groundwater. The formation of Ca-UO_2-CO_3 complexes is known to limit microbial reduction of U^{VI} to U^{IV};[37] however, the effect of these complexes on the abiotic reduction of U^{VI} by Fe^{II} species is largely unknown.

In this study, we examined the potential differences between BioGR and ChemGR with respect to U^{VI} reduction in synthetic groundwater, particularly the speciation, transformation, and stability of the resulting

U^{IV} species using x-ray absorption fine structure (XAFS) spectroscopy and carbonate extraction. We hypothesized that BioGR and ChemGR affect differently the speciation, transformation, and stability of U^{VI} reduction products based on the presence of organic ligands and presumed differences in surface properties.[32]

MATERIALS AND METHODS

Synthesis of GRs

Experiments were conducted using biogenic and abiotic hydroxycarbonate GR, because hydroxycarbonate GR is the most prevalent form in natural systems;[9, 10, 38] moreover, preliminary experiments demonstrated that hydroxycarbonate GR is more stable than hydroxychloride GR or hydroxysulfate GR in our synthetic groundwater (data not shown), consistent with previous studies of GR stability.[39, 40] The ChemGR was synthesized using the coprecipitation method described by Etique et al.[23] Briefly, 9.341 g of ferrous sulfate heptahydrate and 4.789 g of ferric sulfate hydrate were dissolved in 100 mL of deoxygenated deionized water in an anoxic glovebox (N_2/H_2, 95%/5%), resulting in a ferric molar fraction ($x = [Fe^{III}]/([Fe^{II}] + [Fe^{III}])$) of 0.33. Then 100 mL of a basic solution of 1008 mM NaOH and 588 mM Na_2CO_3 was added to the Fe^{II}–Fe^{III} solution, corresponding to a $[OH^-]/([Fe^{II}] + [Fe^{III}])$ ratio of 2 and $[CO_3^{2-}]/([Fe^{II}] + [Fe^{III}])$ ratio of 7/6. A bluish-green precipitate appeared immediately. The solids were collected by centrifugation and washed three times with sterile, anoxic deionized (DI) water to remove any soluble reactants.

The BioGR was obtained from the bioreduction of lepidocrocite by *Shewanella putrefaciens* CN32 as described by O′Loughlin et al.[35] BioGR was pasteurized (65 °C for 1 h) to eliminate the potential for microbial reduction of U^{VI} (a control reactor with unpasteurized BioGR was also examined). The BioGR solids were collected by centrifugation and were repeatedly washed with sterile, anoxic water to promote removal of cells, cell debris, and any soluble reductants. Characterization of the ChemGR and BioGR by powder x-ray diffraction (pXRD) both before and after the washing procedure showed no indication of changes in their crystallographic features (Figure S1). Moreover, control experiments comparing unwashed BioGR and washed BioGR did not show differences in U^{VI} removal or U extraction (Figure S2), indicating the washing procedure didn't affect the reactivity of the BioGR. After the final washing, GRs were re-suspended in sterile deoxygenated CO_2-free deionized water.

Experimental Design

Unless indicated otherwise, experimental setup, execution, and sample preparation were conducted under anoxic conditions—typically in sealed containers in a glovebox with 3–5% H_2 in N_2 (O_2 < 1 ppm in the gas atmosphere). The synthetic groundwater (SGW) used in our experiments was formulated to mimic the composition of uranium-contaminated groundwater at the US DOE Hanford site.[41] The SGW was prepared by mixing three stock solutions (14.4 mM $NaHCO_3$ and 1.6 mM $KHCO_3$; 5.1 mM $MgSO_4$ and 1.2 mM $CaSO_4$; and 8.8 mM $CaCl_2$) in DI-water to obtain the following composition: 1.44 mM $NaHCO_3$, 0.16 mM $KHCO_3$, 0.51 mM $MgSO_4$, 0.12 mM $CaSO_4$, and 0.88 mM $CaCl_2$. No precipitates were observed in the SGW and the pH was 7.9. The experimental system consisted of 50-mL polypropylene centrifuge tubes with screw caps containing 40 mL of SGW, U^{VI}, and GR. SGW and U^{VI} were premixed overnight to reach equilibrium before adding the GR slurry. The DI-control system contained 40 mL of anoxic DI-water, U^{VI}, and GR. Reactions were initiated by spiking with the GR slurry to provide final Fe^{II} and U^{VI} concentrations of 60 mM and 1 mM, respectively. Then the slurry was mixed thoroughly with a rotator at 50 rpm. All the reactions and samples were prepared in duplicate. At selected times, an aliquot of the suspension was centrifuged, and the U^{VI} concentration in the supernatant was measured to determine the kinetics of U^{VI} removal from solution. The extractability of U^{IV} was examined using a carbonate extraction approach via the addition of 0.1 mL of suspension to 0.9 mL of anoxic 2 M Na_2CO_3. After 24 h, the mixture was centrifuged, and the supernatant was retained for measurement of extracted U. Our preliminary assessment of carbonate extraction efficiency indicated that 1.8 M carbonate was sufficient to extract the labile U associated with GR solids under our experimental conditions and the extraction efficiency did not change after 24 h of extraction (Figure S3). The solid samples used for XAFS analysis were collected by filtration on 0.22-μm nylon filters, and then the filter membrane with the hydrated solids was sealed with 8.4-μm-thick Kapton film and tape under anoxic conditions.

Analytical procedures

The pXRD analysis was performed with a Rigaku MiniFlex x-ray diffractometer with Ni-filtered Cu Kα radiation. Samples for pXRD analysis were collected by filtration on 25-mm, 0.22-μm nylon filters and covered with 8.4-μm-thick Kapton film under anoxic conditions. The samples were scanned between 5° and 80° 2θ at a speed of 2.5° 2θ min^{-1}. The pXRD patterns were analyzed with the JADE 6 software package (MDI, Livermore, California). The Fe(II) concentrations in the reactors and GR stock suspensions were determined using the ferrozine method[42] after digestion with anoxic 2 M HCl in the anoxic glovebox. Samples for measurement of aqueous U in GR suspensions were prepared via centrifugation at 13,000 *g* for 2 min inside an anoxic glovebox with 3–5% H_2 in N_2 (O_2 < 1 ppm in the gas atmosphere). Preliminary experiments didn’t show any difference in aqueous U concentrations between samples centrifuged then filtered through 0.22 μm membrane filters and samples only centrifuged, therefore subsequent samples were only centrifuged. The aqueous and extracted U^{VI} concentrations in the reactors were measured using a Chemchek kinetic phosphorescence analyzer (KPA-11) following the procedure developed by Sowder et al. and Dong et al.[43, 44] Selected samples were also analyzed by inductively coupled plasma-optical emission spectroscopy (ICP-OES). The data obtained by these two methods were consistent, with a difference always less than 6%. The speciation of U in the solid phases of the reactors was analyzed by x-ray absorption spectroscopy at sectors 10-ID and 10-BM of the Advanced Photon Source, using a setup described in more detail in the Supporting Information (SI).[34-36] Briefly, x-ray absorption near-edge spectroscopy (XANES) and extended x-ray absorption fine structure (EXAFS) scans at the U L_{III} edge (17,166 eV) were collected in quick scanning mode (3 min each). The final spectrum was produced by averaging 30–50 quick EXAFS scans. The data were processed using ATHENA, and the contributions of distinct U^{IV} species in the EXAFS spectra were quantified using linear combination (LC) fitting.[45] Previously measured spectra from a nanoparticulate uraninite standard and U^{IV}-carbonate complexes were used as end members.[6] Additional details of the XAFS data collection and analysis are provided in the SI.

RESULTS AND DISCUSSION

U^{VI} removal by GR

U^{VI} was rapidly removed from solution in both the ChemGR and BioGR systems (Figure 1). Since the total U concentration in the systems were supersaturated with respect to schoepite, it is possible that the loss of U^{VI} from solution could be due in part to precipitation of a U^{VI} phase such as schoepite. However the aqueous U^{VI} concentrations remained stable at ~1000 μM in the control systems without GR (Figure 1) and there was no visual indication of precipitate formation over the period of observation; thus the rapid initial removal of U^{VI} can be attributed to uptake by GR. In the DI-water control system, over 99% of U^{VI} was removed within 5 min by ChemGR and BioGR, which is comparable to the results reported by O'Loughlin et al.[35] In the SGW system, U^{VI} was also rapidly removed from solutions by ChemGR and BioGR, indicating both GRs are likely to be effective for removal of U^{VI} from groundwater even in the presence of calcium and carbonate. There was no significant difference in the kinetics of U^{VI} removal from solution between ChemGR and BioGR. This is similar to the result in Remy et al., which showed no significant difference between ChemGR and BioGR with respect to Hg^{II} reduction.[33]

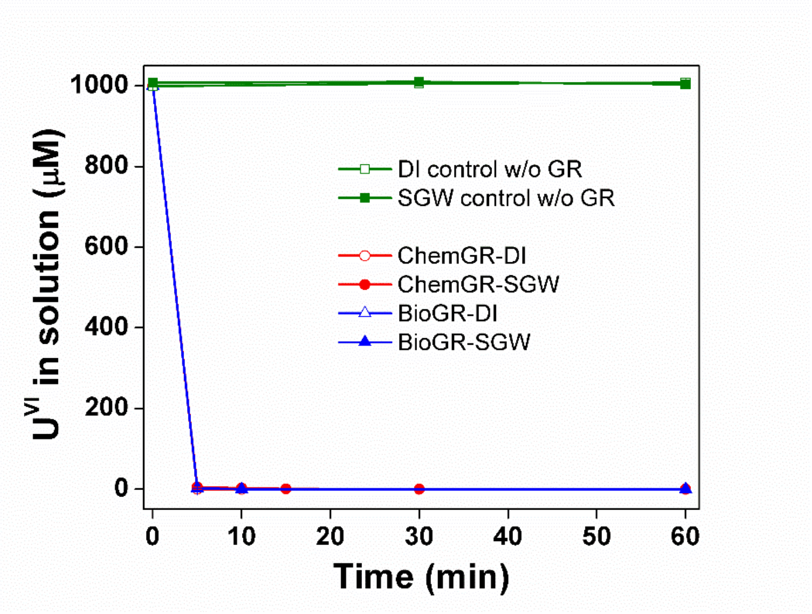

Figure 1. Removal of U^{VI} from solution by ChemGR and BioGR in deionized water (DI) and synthetic groundwater (SGW) systems.

U^{VI} Is Reduced to U^{IV} by GR

U L_{III} edge XANES spectra (Figure 2) show that under all experimental conditions the U associated with the solids is predominantly U^{IV}. The edge energy position and the spectral shape of all XANES spectra are similar to the U^{IV} standard, indicating that over 95% of the U in the solid phase is U^{IV}. Small amounts of U^{VI} were observed only in the 1 h BioGR samples from the DI-water and SGW systems (small shoulder near 17,180 eV in Figure 2), which were quantified as ~17% of solid-phase U based on LC fits of the XANES data with U^{IV} and U^{VI} standards (analysis not shown). Together with the similar and rapid uptake kinetics in all systems (Figure 1), the XANES results suggest that an adsorption step occurring on the timescale of minutes is followed by a fast (<1 h) reduction of U^{VI} to U^{IV}. Similar uptake profiles (i.e., rapid uptake followed by reduction) have been observed in previous studies with GR, as well as with other Fe^{II} phases.[35, 36, 46-48]

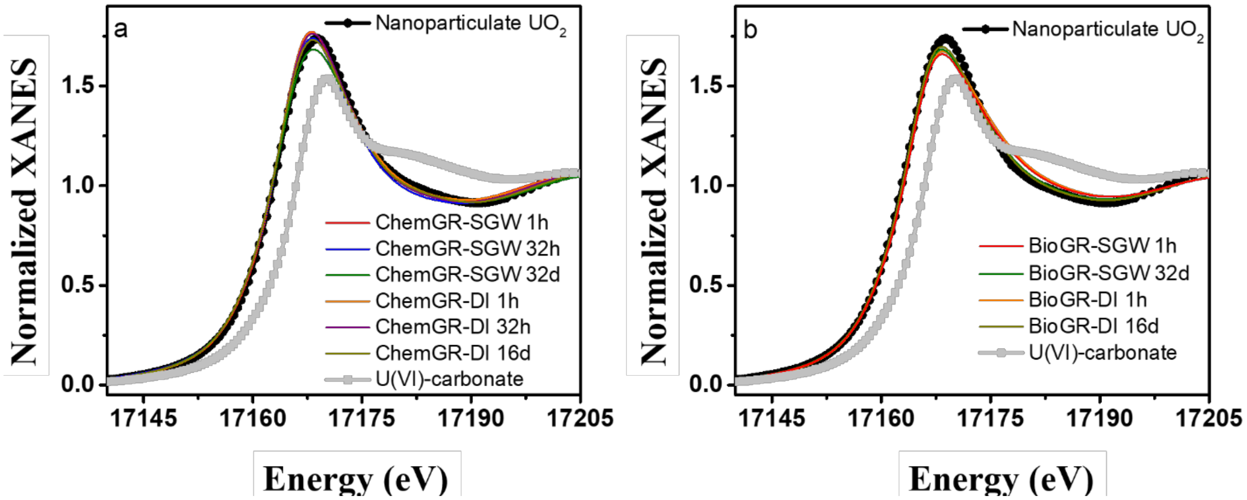

Figure 2. U L_{III} edge XANES spectra for (a) ChemGR and (b) BioGR at various times in deionized water (DI) or synthetic groundwater (SGW) systems compared with U^{IV} and U^{VI} standards.

Extraction of U by Carbonate in the ChemGR and BioGR Systems

Carbonate has been shown to extract U associated with mineral and biological solids, in both the U^{VI} [49-51] and the U^{IV} valence states.[5, 51] The latter studies also showed that U^{IV} is less extractable when present as uraninite relative to the more labile monomeric species (e.g., adsorbed or ligand-complexed U^{IV}). The XANES results indicate that U^{VI} was reduced to U^{IV} in both the ChemGR and BioGR reactors and we used a 1.8 M carbonate extraction method to evaluate the relative stability of U^{IV} in these two systems. As shown in Figure 3, the pool of labile (i.e., carbonate-extractable) U is significantly larger in the BioGR system than in the ChemGR system. The pools of extractable U in both systems gradually decreased over time until they reached steady state, suggesting that the U^{IV} species aged to a more stable form over a period of days. For instance, in SGW, about 85% of the U in the solids could be extracted in the BioGR system after 24 h, but after 4 d of reaction the carbonate-extractable U decreased to 70% and remained unchanged over the following 28 d. Similarly, in the ChemGR system about 50% of U in the solids could be extracted after 24 h, only 30% after 4 d, and only 10% after the system reached steady state at 16 d. In the reactors with BioGR, more U was extractable in SGW than in the DI-water control, which suggests that the presence of calcium and carbonate during U^{VI} reduction by BioGR increased the extractability of U in the system. In contrast, the ChemGR systems showed no significant difference in U extractability between the DI-water and SGW solution conditions.

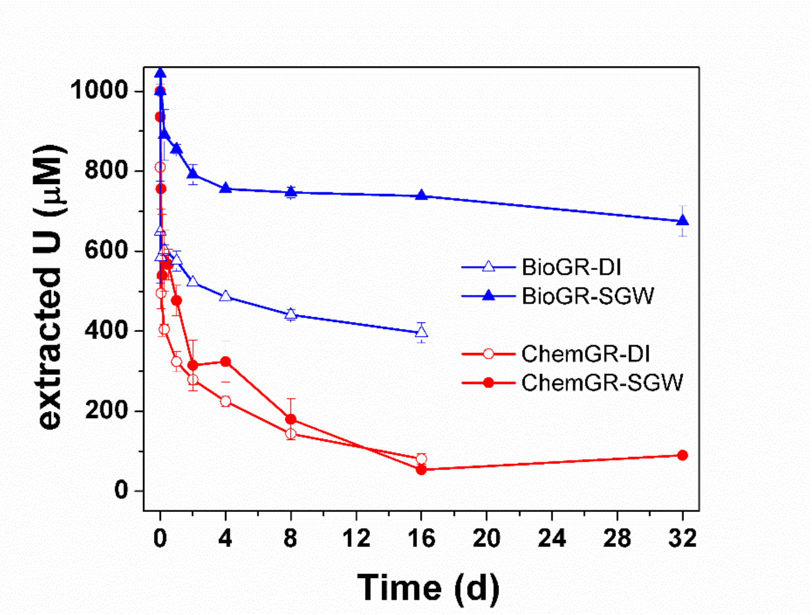

Figure 3. Changes in carbonate-extractable U over time in ChemGR and BioGR systems with deionized water (DI) or synthetic groundwater (SGW). The error bars denote the standard error of measurements made on duplicate bottles.

When interpreting the lability of solid-phase U^{IV} to carbonate extraction we need to consider the valence state of U released in solution. Stoliker et al.[5] concluded that anoxic carbonate extractions of U^{IV} resulted in dissolved U^{VI} and suggested that the change in thermodynamic conditions promoted back-transfer of electrons from U^{IV} to Fe^{III} in the same sediment matrix that originally reduced U^{VI}. It is possible that U^{IV} reoxidized to U^{VI} here as well, since the 1.8 M Na_2CO_3 added during extraction significantly increased the pH values in the SGW ChemGR and BioGR systems from 8.4 to 11.9 and from 8.0 to 11.8, respectively, and the *E*h increased from -674 mV to -471 mV, and from -706 mV to -507 mV, respectively. Figure S4 presents the XANES data from the carbonate extraction supernatants, showing that predominantly U^{VI} was released in solution. We observed the same U concentrations by kinetic phosphorescence analysis before and after oxidation of the extraction supernatants in air (data not shown), also showing that predominantly U^{VI} was present in the extracts. Both of the above suggest that the change in solution conditions caused by the addition of carbonate resulted in the reoxidation of solids-associated U^{IV} leading to the release of U^{VI}. However, the possibility that U^{IV} was first removed from the solids as U^{IV}-carbonate complexes and then reoxidized as a soluble species by contact with Fe^{III} cannot be excluded by the current data. Thus, the data in Figure 3 may indicate either susceptibility of the reduced U^{IV} phases to oxidation under the conditions of the extractions or susceptibility of U^{IV} to complexation by carbonate, if the latter is the rate determining step in the observed oxidative release. Regardless of the actual oxidation mechanism during extraction, the different extractability of U^{IV} in the ChemGR and BioGR systems suggest differences in the initial U^{IV} speciation of U^{IV} produced in these two systems, as confirmed by the EXAFS results below.

U Speciation in the ChemGR and BioGR Systems

The observed differences in U^{IV} extractability suggest differences in U^{IV} speciation between the ChemGR and BioGR systems. We used EXAFS spectroscopy to examine the molecular structure around the U^{IV} atoms in both systems. In the ChemGR system, the EXAFS spectra show systematic trends as a function of reaction time, in both the SGW (Figure 4) and the DI-water control (Figure S5) systems. Specifically, the Fourier transform (FT) of the EXAFS data for the 1-h reaction time samples lacks significant amplitude around $R + \Delta = 3.7$ Å, where the U coordination shell contributes in the uraninite standard. The experimental spectra from the 1 h samples closely resemble that of a previously characterized U^{IV}-carbonate complex produced by bacteria,[6] both in the phase and amplitude of the $\chi(k)$ data, as well as in the features of the FT (Figures 4 and S5). The fits of the data confirm the presence of U^{IV}-carbonate coordination (details in Figures S6-S8 and Table S1), suggesting that a U^{IV}-carbonate complex is the initial species resulting from reduction of U^{VI} by ChemGR. It is possible that these complexes occupy the interlayer space in the GR structure, are adsorbed as ternary =FeO-carbonate-U^{IV} complexes at edge sites of the Fe hydroxide layer, or are outer-sphere associated with the GR surface; however, these possibilities cannot be discerned by the EXAFS data.. There is a consistent increase in the amplitude of the U peak with reaction time, and the samples at 16 d and 32 d approach the nanoparticulate uraninite standard. The real part of the FT EXAFS also approaches the uraninite standard over the duration of the reaction, showing an increase in the U signal and a slight decrease in the bond distance of O in the first shell (Figures S9 and S10). These spectral trends suggest that initially the entire budget of U associated with the solid phase of ChemGR is predominantly in a U^{IV}-carbonate complex, which then gradually transforms to a predominant nanoparticulate uraninite phase over the 32-d reaction period.

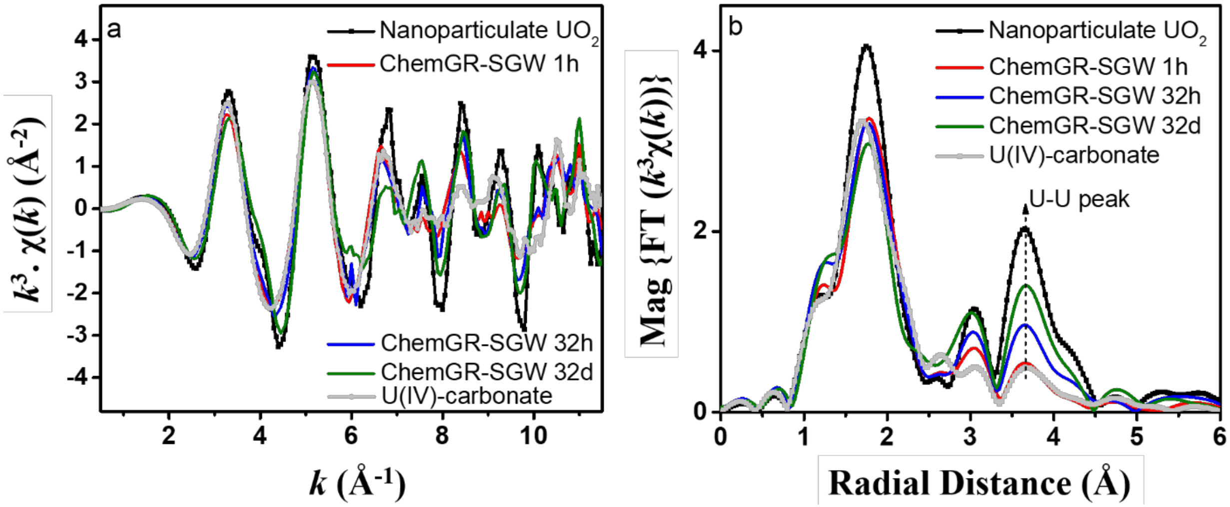

Figure 4. U L_{III} edge (a) k^3-weighed EXAFS data and (b) Fourier transformed (FT) EXAFS spectra for ChemGR in the synthetic groundwater (SGW) system after 1 h, 32 h, and 32 d, compared with nanoparticulate uraninite and U^{IV}-carbonate standards. The vertical dashed line indicates the peak in the FT EXAFS resulting from the contribution of the U shell in uraninite. The FT is within the data range k = 2.2–10.4 $Å^{-1}$ using 1.0-$Å^{-1}$-wide Hanning windowsills. Significant spectral similarity is evident between the 1 h sample (red line) and a previously characterized U^{IV}-carbonate complex[6] (grey symbols).

The proportions of solid-phase U species suggested by the qualitative analysis were quantified by LC fitting of the EXAFS spectra. We used previously characterized spectra of nanoparticulate uraninite and a U^{IV}-carbonate complex as end members.[6] The data from the ChemGR systems after 1 h, 32 h and 32 d indicate an increasing contribution of the uraninite phase from 8% to 25% to 77% in SGW and from 24% to 33% to 75% in DI-water (Table S2) and a general trend of a higher proportion of uraninite in the DI-water system compared to the SGW system. However, the difference between the two solution conditions is within the uncertainty associated with the LC analysis (~10%), so uraninite formation in the SGW system is inhibited only within the first hour of reaction time. Similar proportions of adsorbed U^{IV} species and nanoparticulate uraninite were observed in the previous study by Latta et al.,[36] in which chemogenic carbonate-GR was reacted with U^{VI} in DI water for 3–4 days (58% uraninite, LC analysis shown in Figure S11). Taken together, the carbonate extraction data (Figure 3) and the LC analysis support a reaction sequence whereby an initial labile U^{IV}-carbonate species is formed following the electron transfer between ChemGR and adsorbed U^{VI}, which then transforms over time to a more stable (i.e., less extractable) nanoparticulate uraninite form.

The behavior of U^{IV} in the BioGR system is significantly different compared to its behavior in the ChemGR system. The U EXAFS data in the BioGR system are the same for the 16-d and 32-d samples in DI water and SGW (Figure S12), which indicates lack of evolution of the U^{IV} species over the reaction period and lack of dependence of the U^{IV} product on solution conditions. The 32-d BioGR-SGW spectra were highly reproducible for the pasteurized sample and the unpasteurized control, which suggests that biological processes did not play a role in the final U^{IV} speciation. The spectrum with the best signal-to-noise ratio (BioGR-SGW, 32 d) was used for comparison to U^{IV} standards and for structural analysis. The spectra of the standards were collected previously at the same beamline and include nanoparticulate uraninite,[6] aqueous U^{IV} obtained by dissolving UO_2 in 0.5 M sulfuric acid,[52] monomeric U^{IV} complexed to magnetite,[52] U^{IV} complexed to phosphate, and U^{IV} complexed to biomass without phosphate.[6, 53] Data comparisons (not shown) between the BioGR sample and the aqueous U^{IV} standard or U^{IV} complexed to magnetite indicated significant differences, allowing exclusion of an outer-sphere surface complexation mechanism or the inner-sphere complexation mechanism with increased U^{IV}-O coordination (9–10 O atoms) such as that observed previously for magnetite.[52] The position and amplitude of the main O peak in the FT EXAFS of the BioGR sample (Figure 5) is similar to that in the standards with 8-coordinated U^{IV}. The lack of a U-U backscattering signal near R + Δ = 3.8 Å in the BioGR data (Figure 5) excludes nanoparticulate uraninite as the predominant U^{IV} phase (in other words, <10% of total U may be present as uraninite). When compared to the spectra of U^{IV} associated with biomass in the presence and absence of phosphate,[6] the BioGR spectrum lacks the features assigned previously to complexation of U^{IV} by a phosphate or a R-COO group (indicated by P and C in Figure 5). The BioGR spectrum is nearly identical to that of U^{IV} produced in a previous study by reacting U^{VI} in TAPS buffer with chemically synthesized GR.[36]

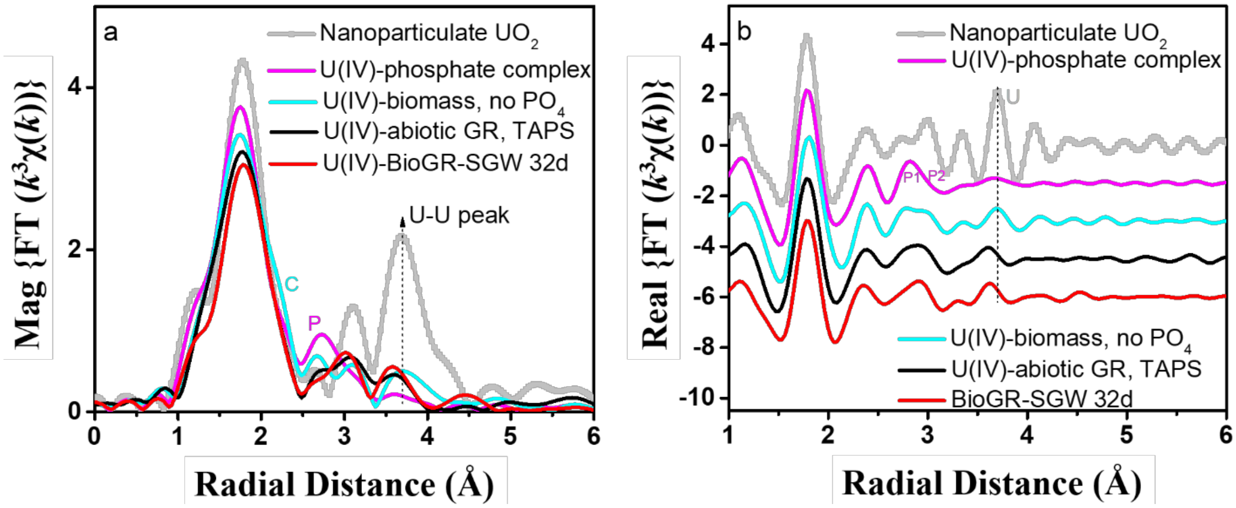

Figure 5. Comparison of the EXAFS data from the BioGR system to U^{IV} standards. (a) Magnitude of the Fourier transformed k^3-weighed EXAFS data; (b) real part of the Fourier transformed k^3-weighed EXAFS data. The shoulder in the first shell of the FT magnitude spectrum of the U^{IV}-biomass standard, representing the contribution of C, and the peak where P atoms contribute in the spectrum of the U^{IV}-phosphate standard are indicated, as determined from previous analyses.[6] The vertical dashed line indicates the signal from the U backscattering atom in uraninite. P1 and P2 indicate the approximate positions of the signals from the bi-

and mono-dentate bound phosphate groups. The spectrum of U^{IV} in the abiotic GR TAPS buffer system is taken from Latta et al.[36] The Fourier transform is within the data range $k = 2.2–10.4$ Å^{-1} using 1.0-Å^{-1}-wide Hanning windowsills.

In light of the similarity between the U+BioGR data and the data from U+chemical GR in the TAPS buffer from Latta et al.,[36] the EXAFS model from that work was applied to fit the U+BioGR data. The model included a near-neighbor O shell, an Fe shell, and an outer O shell, and produced the best simultaneous fit of the data at k-weights of k^1, k^2, and k^3 in the Fourier transform (Figure S13 and Table S3). The refined parameters show that the average U-O distance in the BioGR system is 2.35 ± 0.01 Å, which is similar to the U-O distance in 8-coordinated U^{IV} species such as nanoparticulate uraninite (2.32 ± 0.01 Å) and phosphate-complexed U^{IV} (2.33 ± 0.01 Å), but significantly shorter than that of 9–10 coordinated U^{IV} species such as aqueous U^{IV} or U^{IV} adsorbed to the =FeO sites in magnetite (2.42 ± 0.02 Å).[52] The lower amplitude of the O-shell peak in the BioGR data relative to nanoparticulate uraninite or phosphate-complexed U^{IV} results from a slight decrease in average coordination number and a slight increase in the disorder (Debye-Waller factor) relative to the standards. Attempts to model the BioGR data with the second shell U paths used to fit the nanoparticulate uraninite data indicated that the signal between $R + \Delta = 3.0–4.0$ Å is inconsistent with U. Similarly, EXAFS modeling efforts based on the ningyoite $CaU^{IV}(PO_4)_2$ structure representing U^{IV}-phosphate complexation were also unsuccessful.[6, 54]

The refined structural model with an O, Fe, and O coordination shells is consistent with adsorption of U^{IV} to the brucite layer in the GR structure or possibly to other Fe transformation products in the system, rather than complexation to the carbonate anions in the interlayer or to residual biological components in the BioGR system. Association of U^{IV} with Fe redox products has been observed before in laboratory and natural systems.[3, 55] The nearly identical U EXAFS data in the BioGR system here and in chemical GR systems studied previously[36] (Figure 5) also suggest U^{IV} association with the iron oxides rather than with a biological component. However, it should be noted that the adsorbed U^{IV} species in the carbonate GR reactors of Latta et al.[36] were observed only in the presence of TAPS buffer, whereas significant nanoparticulate uraninite formation occurred in DI water (LC fit shown in Figure S11). Thus, although carbonate GRs adsorb U^{IV} atoms at the ≡FeO sites, the stability of adsorbed U^{IV} with respect to desorption and uraninite formation appears dependent on the presence of residual organic components or buffers. Recent studies have also identified U^{IV}-organic matter complexation in field samples.[56] This indirect effect of organic molecules on the stability of reduced U is important in an environmental context and needs to be elucidated in further studies with controlled addition of organic matter. Stabilization of non-uraninite U^{IV} in biogenic GR reactors was also observed in the previous study by O'Loughlin et al.[35] Although the EXAFS data were interpreted at the time as a highly disordered uraninite phase, a comparison between the BioGR data here and in the previous study[35] reveals that the data are the same within measurement uncertainty (Figure S14). Thus, the analysis and conclusions presented above can be directly applied to the data in O'Loughlin et al.[35] An EXAFS model with O, Fe, and O shells that is conceptually similar to the U^{IV} adsorption mechanism determined in our study was also fit to the data from monomeric U^{IV} in magnetite solids at low U:magnetite ratios.[52] However, the U-O and U-Fe distances refined for the BioGR samples are significantly shorter than in the U^{IV}-magnetite complexes (2.35 Å vs. 2.42 Å, and 3.49 Å vs. 3.59 Å, respectively). This indicates a different binding mechanism of U^{IV} to BioGR relative to that in magnetite and suggests that the arrangement of the ≡FeO sites plays a significant role in the complexation of U^{IV} to iron oxide surfaces.

Based on the speciation for the BioGR and ChemGR systems, the persistence of adsorbed U^{IV} species in the BioGR system over the 32-d reaction period can explain their consistently high extractability with carbonate (Figure 3), whereas the transformation of adsorbed U^{IV} to uraninite in the ChemGR system can explain the significant decrease in U^{IV} extractability over time. Figure 3 also reveals a relatively higher extractability of U^{IV} in SGW compared to the DI-water samples within the BioGR system. However, the EXAFS data show no significant differences in the U spectra between the BioGR reactors (Figure S12).

This suggests that the molecular structure of U alone cannot explain the observed differences in U extractability. It is possible that components of the SGW solution affect U speciation in the BioGR system in a way that is not apparent in the EXAFS spectra (e.g., outer-sphere complexation) or that the different solution compositions affect particle size or aggregation and thus the ability of carbonate to reach and extract the U^{IV} complexes. It is also possible that interaction between the biological components and DI water versus SGW affects the efficiency of the carbonate extraction of the same U^{IV} species.

Environmental implications

The reduction of soluble uranyl to less soluble U^{IV} species is a key process in the biogeochemistry of U in both natural and engineered environments under suboxic to anoxic conditions. However, U is not typically present at high enough concentrations to control the redox state of a given environment, therefore the reduction of U^{VI} is often coupled to that of a more abundant redox active element such as Fe. As previously mentioned, GRs have been identified in Fe^{III}/Fe^{II} transitions zones in a variety of natural environments[9, 11-17] and engineered systems such as Fe^0 permeable reactive barriers[57, 58] where due to their effectiveness as reductants for U^{VI}, they may play a role in U speciation thereby impacting U fate and transport in these environments. Our results showing differences in the speciation of the U^{IV} products resulting from the reduction of U^{VI} by biogenic GR compared to chemogenic GR as well as previous studies demonstrating differential reactivity between biogenic and chemogenic Fe^{II} phases,[32, 33, 47 59] highlight the importance of identifying the processes leading to the in situ formation of these reactive species in understanding their potential role in contaminant fate and transport. However, contaminant speciation also plays a critical role. Calcium and carbonate are ubiquitous components in U-contaminated groundwater. According to equilibrium thermodynamic calculations, U^{VI} can form stable ternary calcium-uranyl-carbonate complexes in groundwater that contains calcium and carbonate.[44] Theoretically, the stable ternary complex of U^{VI} is a less thermodynamically favorable electron acceptor than the uranyl hydroxyl complex, which leads to a decrease in the rate and extent of U^{VI} reduction.[44, 50] Previous studies demonstrated that the presence of calcium and carbonate at millimolar concentrations can cause a significant decrease in the rate and extent of bacterial U^{VI} reduction.[37,60] However, our results show that the potential for formation of ternary calcium-uranyl-carbonate complexes did not have an observable effect on the rate or extent of reduction of U^{VI} by ChemGR and BioGR in synthetic groundwater containing calcium and carbonate. Thus, GRs (whether synthetic or the product of microbial Fe redox transformations) could provide a more effective means of reducing the concentration of uranium in contaminated groundwater than anaerobic U^{VI}-reducing bacteria.

ACKNOWLEDGEMENTS

The authors thank Carolyn Steele and the anonymous reviewers for their thoughtful reviews of the manuscript. This research was supported by the National Natural Science Foundation of China (41303084 and 41521001); the 111 Program (State Administration of Foreign Experts Affairs & the Ministry of Education of China, grant B18049); the Fundamental Research Funds for the Central Universities, China University of Geosciences-Wuhan (CUG170402 and CUG170104); and the Subsurface Science Scientific Focus Area (SFA) at Argonne National Laboratory funded by the Subsurface Biogeochemical Research Program, Office of Biological and Environmental Research, Office of Science, U.S. Department of Energy (DOE), under contract DE-AC02-06CH11357. Use of the Advanced Photon Source was supported by the U.S. Department of Energy, Office of Science, Office of Basic Energy Sciences. We thank the MRCAT/EnviroCAT beamline staff at the Advanced Photon Source for assistance during XAFS data collection. MRCAT/EnviroCAT operations are supported by DOE and the MRCAT/EnviroCAT member institutions.

SUPPORTING INFORMATION AVAILABLE

The Supporting Information includes pXRD patterns of ChemGR and BioGR, a comparison of the reactivity of washed and unwashed BioGR, assessments of carbonate extraction efficiency, details of XAFS data collection and analysis, and supplemental XAFS spectra. This material is available free of charge via the Internet at http://pubs.acs.org.

REFERENCES

(1) Riley, R. G.; Zachara, J. M. *Chemical contaminants on DOE lands and selection of contaminant mixtures for subsurface science research*; U.S. Department of Energy: Washington, DC, 1992.

(2) O'Loughlin, E. J.; Boyanov, M. I.; Antonopoulos, D. A.; Kemner, K. M., Redox processes affecting the speciation of technetium, uranium, neptunium, and plutonium in aquatic and terrestrial environments. In *Aquatic Redox Chemistry*, Tratnyek, P. G., Grundl, T.J., Haderlein, S.B., Ed. 2011; pp 477-517.

(3) Kelly, S. D.; Kemner, K. M.; Carley, J.; Criddle, C.; Jardine, P. M.; Marsh, T. L.; Phillips, D.; Watson, D.; Wu, W. M. Speciation of uranium in sediments before and after in situ biostimulation. *Environ. Sci. Technol.* **2008,** *42* (5), 1558-1564.

(4) Bargar, J. R.; Williams, K. H.; Campbell, K. M.; Long, P. E.; Stubbs, J. E.; Suvorova, E. I.; Lezama-Pacheco, J. S.; Alessi, D. S.; Stylo, M.; Webb, S. M.; Davis, J. A.; Giammar, D. E.; Blue, L. Y.; Bernier-Latmani, R. Uranium redox transition pathways in acetate-amended sediments. *Proc. Natl. Acad. Sci. U. S. A.* **2013,** *110* (12), 4506-4511.

(5) Stoliker, D. L.; Campbell, K. M.; Fox, P. M.; Singer, D. M.; Kaviani, N.; Carey, M.; Peck, N. E.; Bargar, J. R.; Kent, D. B.; Davis, J. A. Evaluating chemical extraction techniques for the determination of uranium oxidation state in reduced aquifer sediments. *Environ. Sci. Technol.* **2013,** *47* (16), 9225-9232.

(6) Boyanov, M. I.; Fletcher, K. E.; Kwon, M. J.; Rui, X.; O'Loughlin, E. J.; Loffler, F. E.; Kemner, K. M. Solution and microbial controls on the formation of reduced U(IV) species. *Environ. Sci. Technol.* **2011,** *45* (19), 8336-8344.

(7) Latta, D. E.; Kemner, K. M.; Mishra, B.; Boyanov, M. I. Effects of calcium and phosphate on uranium(IV) oxidation: Comparison between nanoparticulate uraninite and amorphous U^{IV}-phosphate. *Geochim. Cosmochim. Acta* **2016,** *174*, 122-142.

(8) Boyanov, M. I.; Latta, D. E.; Scherer, M. M.; O'Loughlin, E. J.; Kemner, K. M. Surface area effects on the reduction of U^{VI} in the presence of synthetic montmorillonite. *Chem. Geol.* **2017,** *464*, 110-117.

(9) Zegeye, A.; Bonneville, S.; Benning, L. G.; Sturm, A.; Fowle, D. A.; Jones, C.; Canfield, D. E.; Ruby, C.; MacLean, L. C.; Nomosatryo, S.; Crowe, S. A.; Poulton, S. W. Green rust formation controls nutrient availability in a ferruginous water column. *Geology* **2012,** *40* (7), 599-602.

(10) Christiansen, B. C.; Balic-Zunic, T.; Dideriksen, K.; Stipp, S. L. S. Identification of green rust in groundwater. *Environ. Sci. Technol.* **2009,** *43* (10), 3436-3441.

(11) Johnson, C. A.; Freyer, G.; Fabisch, M.; Caraballo, M. A.; Kusel, K.; Hochella, M. F. Observations and assessment of iron oxide and green rust nanoparticles in metal-polluted mine drainage within a steep redox gradient. *Environ. Chem.* **2014,** *11* (4), 377-391.

(12) Trolard, F.; Génin, J. M. R.; Abdelmoula, M.; Bourrié, G.; Humbert, B.; Herbillon, A. Identification of a green rust mineral in a reductomorphic soil by Mössbauer and Raman spectroscopies. *Geochim. Cosmochim. Acta* **1997,** *61* (5), 1107-1111.

(13) Génin, J. M. R.; Bourrie, G.; Trolard, F.; Abdelmoula, M.; Jaffrezic, A.; Refait, P.; Maitre, V.; Humbert, B.; Herbillon, A. Thermodynamic equilibria in aqueous suspensions of synthetic and natural Fe(II)-Fe(III) green rusts: Occurrences of the mineral in hydromorphic soils. *Environ. Sci. Technol.* **1998,** *32* (8), 1058-1068.

(14) Feder, F.; Trolard, F.; Klingelhofer, G.; Bourrie, G. In situ Mossbauer spectroscopy: Evidence for green rust (fougerite) in a gleysol and its mineralogical transformations with time and depth. *Geochim. Cosmochim. Acta* **2005,** *69* (18), 4463-4483.

(15) Bender Koch, C.; Morup, S. Identification of Green Rust in an Ochre Sludge. *Clay Minerals* **1991,** *26* (4), 577-582.

(16) Bearcock, J. M.; Perkins, W. T.; Dinelli, E.; Wade, S. C. Fe(II)/Fe(III) 'green rust' developed within ochreous coal mine drainage sediment in South Wales, UK. *Mineralogical Magazine* **2006,** *70* (6), 731-741.

(17) Root, R. A.; Dixit, S.; Campbell, K. M.; Jew, A. D.; Hering, J. G.; O'Day, P. A. Arsenic sequestration by sorption processes in high-iron sediments. *Geochim. Cosmochim. Acta* **2007,** *71* (23), 5782-5803.

(18) Larese-Casanova, P.; Scherer, M. M. Abiotic transformation of hexahydro-1,3,5-trinitro-1,3,5-triazine (RDX) by green rusts. *Environ. Sci. Technol.* **2008,** *42* (11), 3975-3981.

(19) O'Loughlin, E. J.; Burris, D. R. Reduction of halogenated ethanes by green rust. *Environ. Toxicol. Chem.* **2004,** *23* (1), 41-48.

(20) Williams, A. G. B.; Scherer, M. M. Kinetics of Cr(VI) reduction by carbonate green rust. *Environ. Sci. Technol.* **2001,** *35* (17), 3488-3494.

(21) O'Loughlin, E. J.; Kelly, S. D.; Kemner, K. M.; Csencsits, R.; Cook, R. E. Reduction of Ag(I), Au(III), Cu(II), and Hg(II) by Fe(II)/Fe(III) hydroxysulfate green rust. *Chemosphere* **2003,** *53* (5), 437-446.

(22) Guerbois, D.; Ona-Nguema, G.; Morin, G.; Abdelmoula, M.; Laverman, A. M.; Mouchel, J. M.; Barthelemy, K.; Maillot, F.; Brest, J. Nitrite reduction by biogenic hydroxycarbonate green rusts: Evidence for hydroxy-nitrite green rust formation as an intermediate reaction product. *Environ. Sci. Technol.* **2014,** *48* (8), 4505-4514.

(23) Etique, M.; Zegeye, A.; Gregoire, B.; Carteret, C.; Ruby, C. Nitrate reduction by mixed iron(II-III) hydroxycarbonate green rust in the presence of phosphate anions: The key parameters influencing the ammonium selectivity. *Water Res.* **2014,** *62*, 29-39.

(24) Trolard, F. Fougerite: From field experiment to the homologation of the mineral. *C. R. Geosci.* **2006,** *338* (16), 1158-1166.

(25) Berthelin, J.; Ona-Nguema, G.; Stemmler, S.; Quantin, C.; Abdelmoula, M.; Jorand, F. Bioreduction of ferric species and biogenesis of green rusts in soils. *C. R. Geosci.* **2006,** *338* (6-7), 447-455.

(26) Chaudhuri, S. K.; Lack, J. G.; Coates, J. D. Biogenic magnetite formation through anaerobic biooxidation of Fe(II). *Appl. Environ. Microbiol.* **2001,** *67* (6), 2844-2848.

(27) Pantke, C.; Obst, M.; Benzerara, K.; Morin, G.; Ona-Nguema, G.; Dippon, U.; Kappler, A. Green rust formation during Fe(II) oxidation by the nitrate-reducing *Acidovorax sp.* Strain BoFeN1. *Environ. Sci. Technol.* **2012,** *46* (3), 1439-1446.

(28) Usman, M.; Hanna, K.; Abdelmoula, M.; Zegeye, A.; Faure, P.; Ruby, C. Formation of green rust via mineralogical transformation of ferric oxides (ferrihydrite, goethite and hematite). *Applied Clay Science* **2012,** *64*, 38-43.

(29) Etique, M.; Jorand, F. P. A.; Zegeye, A.; Gregoire, B.; Despas, C.; Ruby, C. Abiotic process for Fe(II) oxidation and green rust mineralization driven by a heterotrophic nitrate reducing bacteria (*Klebsiella mobilis*). *Environ. Sci. Technol.* **2014,** *48* (7), 3742-3751.

(30) O'Loughlin, E. J.; Gorski, C. A.; Scherer, M. M. Effects of phosphate on secondary mineral formation during the bioreduction of akaganeite (β-FeOOH): Green rust versus framboidal magnetite. *Curr. Inorg. Chem.* **2015,** *5* (3), 214-224.

(31) Etique, M.; Jorand, F. P. A.; Ruby, C. Magnetite as a precursor for green rust through the hydrogenotrophic activity of the iron-reducing bacteria *Shewanella putrefaciens*. *Geobiology* **2016,** *14* (3), 237-254.

(32) Zegeye, A.; Etique, M.; Carteret, C.; Ruby, C.; Schaaf, P.; Francius, G. Origin of the differential nanoscale reactivity of biologically and chemically formed green rust crystals investigated by chemical force spectroscopy. *J. Phys. Chem. C* **2014,** *118* (11), 5978-5987.

(33) Remy, P. P.; Etique, M.; Hazotte, A. A.; Sergent, A. S.; Estrade, N.; Cloquet, C.; Hanna, K.; Jorand, F. P. A. Pseudo-first-order reaction of chemically and biologically formed green rusts with Hg^{II} and $C_{15}H_{15}N_3O_2$: Effects of pH and stabilizing agents (phosphate, silicate, polyacrylic acid, and bacterial cells). *Water Res.* **2015,** *70*, 266-278.

(34) O'Loughlin, E. J.; Kelly, S. D.; Cook, R. E.; Csencsits, R.; Kemner, K. M. Reduction of uranium (VI) by mixed iron (II)/iron (III) hydroxide (green rust): Formation of UO_2 nanoparticles. *Environ. Sci. Technol.* **2003,** *37* (4), 721-727.

(35) O'Loughlin, E. J.; Kelly, S. D.; Kemner, K. M. XAFS investigation of the interactions of U(VI) with secondary mineralization products from the bioreduction of Fe(III) oxides. *Environ. Sci. Technol.* **2010,** *44* (5), 1656-1661.

(36) Latta, D. E.; Boyanov, M. I.; Kemner, K. M.; O'Loughlin, E. J.; Scherer, M. Reaction of uranium(VI) with green rusts: Effect of interlayer anion. *Curr. Inorg. Chem.* **2015,** *5* (3), 156-168.

(37) Brooks, S. C.; Fredrickson, J. K.; Carroll, S. L.; Kennedy, D. W.; Zachara, J. M.; Plymale, A. E.; Kelly, S. D.; Kemner, K. M.; Fendorf, S. Inhibition of bacterial U(VI) reduction by calcium. *Environ. Sci. Technol.* **2003,** *37* (9), 1850-1858.

(38) Génin, J. M. R.; Christy, A.; Kuzmann, E.; Mills, S.; Ruby, C. Structure and occurrences of ≪ green rust ≫ related new minerals of the fougérite group, trébeurdenite and mössbauerite, belonging to the hydrotalcite supergroup; how Mössbauer spectroscopy helps XRD. *Hyperfine Interact.* **2014,** *226* (1-3), 459-482.

(39) Refait, P.; Drissi, S. H.; Pytkiewicz, J.; Genin, J. M. R. The anionic species competition in iron aqueous corrosion: Role of various green rust compounds. *Corrosion Science* **1997,** *39* (9), 1699-1710.

(40) Refait, P. H.; Abdelmoula, M.; Genin, J. M. R. Mechanisms of formation and structure of green rust one in aqueous corrosion of iron in the presence of chloride ions. *Corrosion Science* **1998,** *40* (9), 1547-1560.

(41) Lee, J. H.; Fredrickson, J. K.; Kukkadapu, R. K.; Boyanov, M. I.; Kemner, K. M.; Lin, X. J.; Kennedy, D. W.; Bjornstad, B. N.; Konopka, A. E.; Moore, D. A.; Resch, C. T.; Phillips, J. L. Microbial reductive transformation of phyllosilicate Fe(III) and U(VI) in fluvial subsurface sediments. *Environ. Sci. Technol.* **2012,** *46* (7), 3721-3730.

(42) Stookey, L. L. Ferrozine---a new spectrophotometric reagent for iron. *Anal. Chem.* **1970,** *42* (7), 779-781.

(43) Sowder, A. G.; Clark, S. B.; Fjeld, R. A. The effect of sample matrix quenching on the measurement of trace uranium concentrations in aqueous solutions using kinetic phosphorimetry. *J. Radioanal. Nucl. Chem.* **1998,** *234* (1-2), 257-260.

(44) Dong, W.; Brooks, S. C. Determination of the formation constants of ternary complexes of uranyl and carbonate with alkaline earth metals (Mg^{2+}, Ca^{2+}, Sr^{2+}, and Ba^{2+}) using anion exchange method. *Environ. Sci. Technol.* **2006,** *40* (15), 4689-4695.

(45) Ravel, B.; Newville, M. ATHENA, ARTEMIS, HEPHAESTUS: data analysis for X-ray absorption spectroscopy using IFEFFIT. *J. Synchrotron Radiat.* **2005,** *12*, 537-541.

(46) Veeramani, H.; Scheinost, A. C.; Monsegue, N.; Qafoku, N. P.; Kukkadapu, R.; Newville, M.; Lanzirotti, A.; Pruden, A.; Murayama, M.; Hochella, M. F. Abiotic reductive immobilization of U(VI) by biogenic mackinawite. *Environ. Sci. Technol.* **2013,** *47* (5), 2361-2369.

(47) Veeramani, H.; Alessi, D. S.; Suvorova, E. I.; Lezama-Pacheco, J. S.; Stubbs, J. E.; Sharp, J. O.; Dippon, U.; Kappler, A.; Bargar, J. R.; Bernier-Latmani, R. Products of abiotic U(VI) reduction by biogenic magnetite and vivianite. *Geochim. Cosmochim. Acta* **2011,** *75* (9), 2512-2528.

(48) Dodge, C. J.; Francis, A. J.; Gillow, J. B.; Halada, G. P.; Eng, C.; Clayton, C. R. Association of uranium with iron oxides typically formed on corroding steel surfaces. *Environ. Sci. Technol.* **2002,** *36* (16), 3504-3511.

(49) Gu, B.; Liang, L.; Dickey, M. J.; Yin, X.; Dai, S. Reductive precipitation of uranium (VI) by zero-valent iron. *Environ. Sci. Technol.* **1998,** *32* (21), 3366-3373.

(50) Yan, S.; Hua, B.; Bao, Z. Y.; Yang, J.; Liu, C. X.; Deng, B. L. Uranium(VI) removal by nanoscale zerovalent iron in anoxic batch systems. *Environ. Sci. Technol.* **2010,** *44* (20), 7783-7789.

(51) Alessi, D. S.; Uster, B.; Veeramani, H.; Suvorova, E. I.; Lezama-Pacheco, J. S.; Stubbs, J. E.; Bargar, J. R.; Bernier-Latmani, R. Quantitative separation of monomeric U(IV) from UO_2 in products of U(VI) reduction. *Environ. Sci. Technol.* **2012,** *46* (11), 6150-6157.

(52) Latta, D. E.; Mishra, B.; Cook, R. E.; Kemner, K. M.; Boyanov, M. I. Stable U(IV) complexes form at high-affinity mineral surface sites. *Environ. Sci. Technol.* **2014,** *48* (3), 1683-1691.

(53) Fletcher, K. E.; Boyanov, M. I.; Thomas, S. H.; Wu, Q. Z.; Kemner, K. M.; Loffler, F. E. U(VI) reduction to mononuclear U(IV) by *Desulfitobacterium* species. *Environ. Sci. Technol.* **2010,** *44* (12), 4705-4709.

(54) Dusausoy, Y.; Ghermani, N. E.; Podor, R.; Cuney, M. Low-temperature ordered phase of $CaU(PO_4)_2$: Synthesis and crystal structure. *Eur. J. Mineral.* **1996,** *8* (4), 667-673.

(55) Boyanov, M. I.; O'Loughlin, E. J.; Roden, E. E.; Fein, J. B.; Kemner, K. M. Adsorption of Fe(II) and U(VI) to carboxyl-functionalized microspheres: The influence of speciation on uranyl reduction studied by titration and XAFS. *Geochim. Cosmochim. Acta* **2007,** *71* (8), 1898-1912.

(56) Bone, S. E.; Dynes, J. J.; Cliff, J.; Bargar, J. R. Uranium(IV) adsorption by natural organic matter in anoxic sediments. *Proc. Natl. Acad. Sci. U. S. A.* **2017,** *114* (4), 711-716.

(57) Furukawa, Y.; Kim, J. W.; Watkins, J.; Wilkin, R. T. Formation of ferrihydrite and associated iron corrosion products in permeable reactive barriers of zero-valent iron. *Environ. Sci. Technol.* **2002,** *36* (24), 5469-5475.

(58) Phillips, D. H.; Watson, D. B.; Roh, Y.; Gu, B. Mineralogical characteristics and transformations during long-term operation of a zerovalent iron reactive barrier. *J. Environ. Qual.* **2003,** *32* (6), 2033-2045.

(59) McCormick, M. L.; Kim, H. S.; Bouwer, E. J.; Adriaens, P. *Abiotic transformation of chlorinated solvents as a consequence of microbial iron reduction: An investigation of the role of biogenic magnetite in mediating reductive dechlorination,* In: Proceedings of the Thirtieth Mid-Atlantic Industrial and Hazardous Waste Conference-Hazardous and Industrial Wastes. Technomic Publishing Company, Inc., pp 339-348.

(60) Stewart, B. D.; Neiss, J.; Fendorf, S. Quantifying constraints imposed by calcium and iron on bacterial reduction of uranium(VI). *J. Environ. Qual.* **2007,** *36* (2), 363-372.

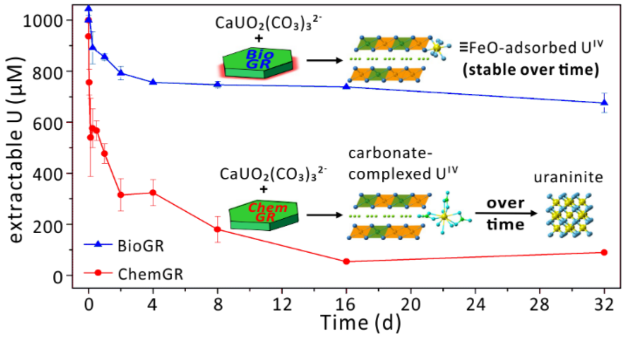

For table of contents only

Supporting Information

U(VI) Reduction by Biogenic and Abiotic Hydroxycarbonate Green Rusts: Impacts on U(IV) Speciation and Stability Over Time

Sen Yan,[1,2*] Maxim I. Boyanov,[2,3] Bhoopesh Mishra,[2,4] Kenneth M. Kemner,[2] and Edward J. O'Loughlin[2*]

1. School of Earth Sciences, China University of Geosciences, Wuhan, China (sen.yan@cug.edu.cn)

2. Biosciences Division, Argonne National Laboratory, Argonne, IL, USA (kemner@anl.gov, oloughlin@anl.gov)

3. Institute of Chemical Engineering, Bulgarian Academy of Sciences, Sofia, Bulgaria (mboyanov@ice.bas.bg)

4. School of Chemical and Process Engineering, University of Leeds, Leeds, UK (b.mishra@leeds.ac.uk)

Number of pages: 17; Number of Tables: 3; Number of Figures: 14

---

[*] Corresponding author (SY) phone: (86) 27-67883033; fax: (86) 27-67883001; e-mail: sen.yan@cug.edu.cn; address: School of Earth Sciences, China University of Geosciences, 388 Lumo Road, Wuhan, China, 430074.

[*] Corresponding author (EJO) phone: (630) 252-9902; e-mail: oloughlin@anl.gov. Corresponding author address: Biosciences Division, Argonne National Laboratory, Building 203, Room E-137, 9700 South Cass Ave., Argonne, IL 60439-4843.

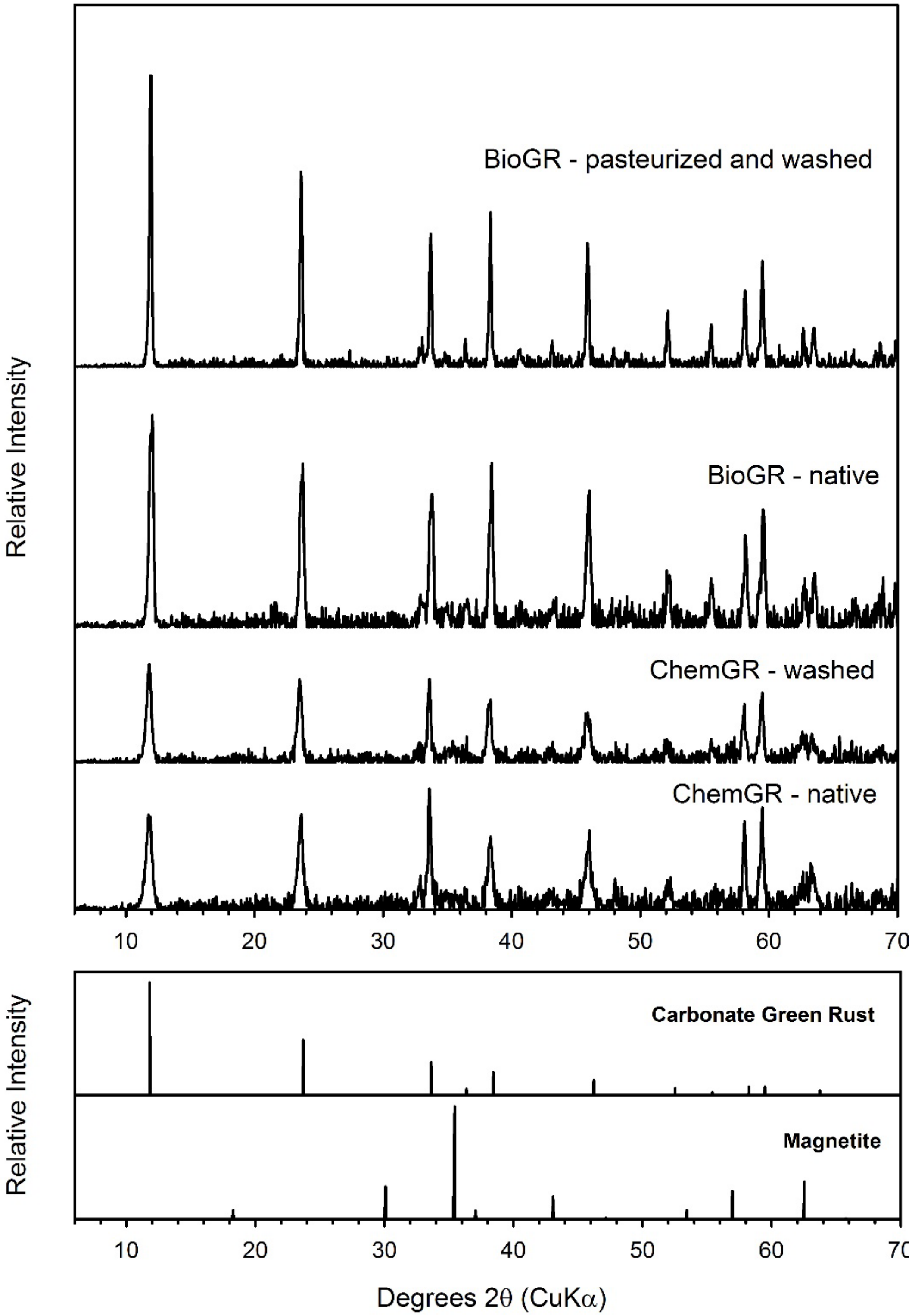

Figure S1. pXRD patterns of ChemGR before and after washing and BioGR before and after pasteurization (65 °C for 1 h) and washing.

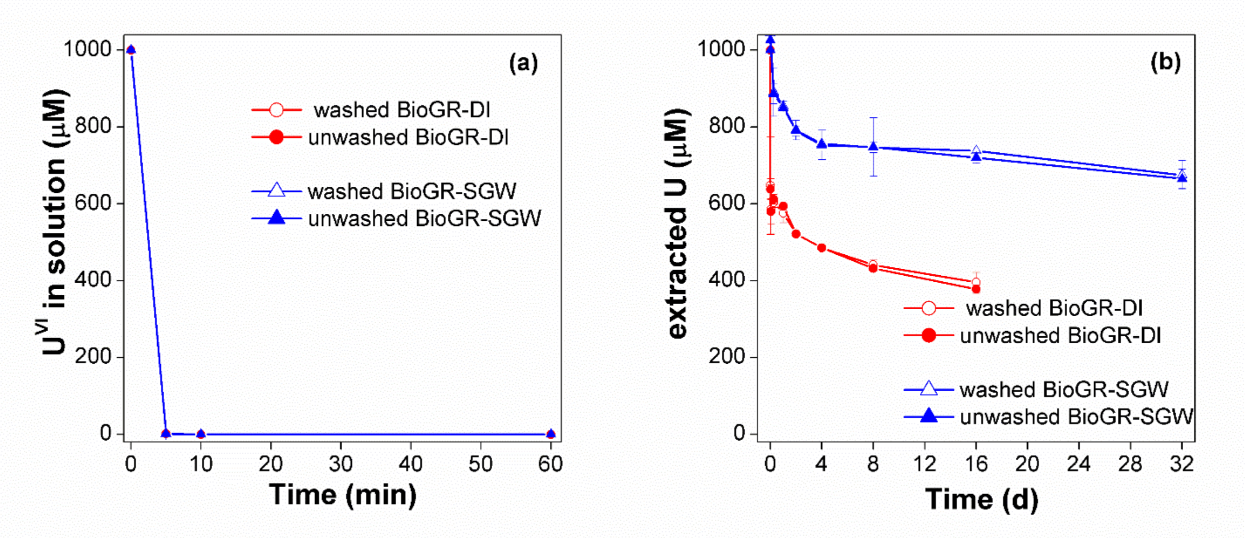

Figure S2. U^{VI} removal (a) and U extraction (b) in the systems with washed and unwashed BioGR.

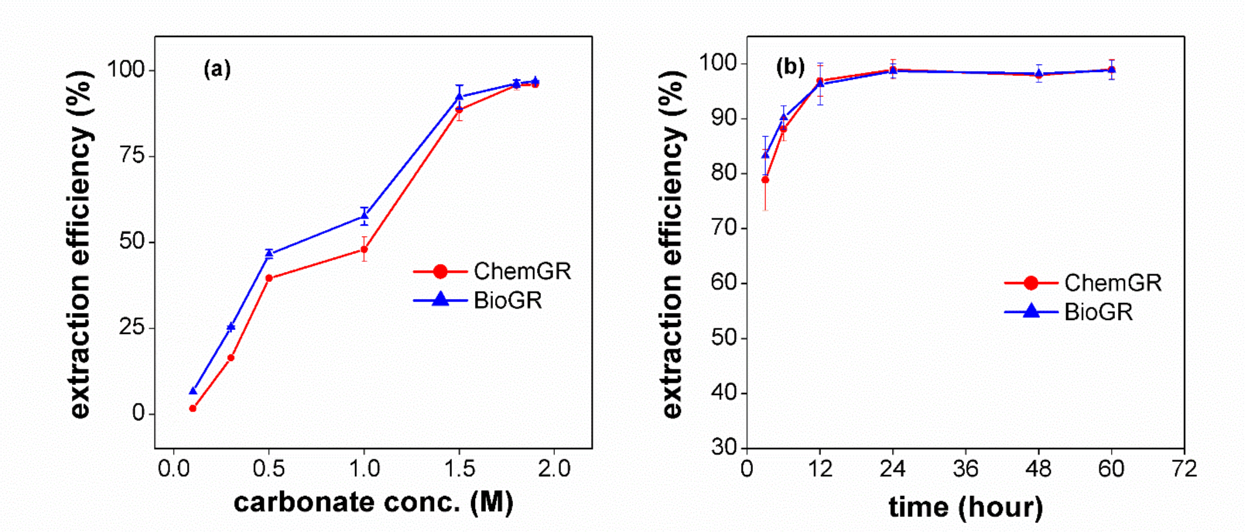

Figure S3. The effects of carbonate concentration (a) and time (b) on U extraction efficiency.

XAFS Data Collection and Analysis

U L_{III} edge (17,166 eV) x-ray absorption spectroscopy measurements were carried out at the MRCAT/EnviroCAT insertion device beamline (Sector 10-ID, Advanced Photon Source).[1] Fluorescence-mode x-ray absorption near edge spectra (XANES) and extended x-ray absorption fine structure (EXAFS) spectra were collected using an Ar-filled ionization chamber. Solution samples were loaded in 3-mm-thick sample holders sealed with x-ray transparent Kapton windows. The reactor solids from the GR systems were collected by filtration through a 0.22-μm filter membrane inside an anoxic glovebox (Coy technologies, 5% H_2/95% N_2, Pd catalyst; O_2 in the gas environment <1 ppm at all times). The hydrated solids were covered with Kapton film, then sealed within two pieces of Kapton tape for the x-ray measurement. All samples were transported in O_2-free containers to the beamline nearby. Spectra were collected at room temperature inside a N_2-purged sample cell. Radiation-induced changes in U speciation were not observed in quick XANES scans (<30 sec each) on a fresh area of the samples. No differences were observed between spectra collected from several different areas on the sample. Therefore, all scans were combined to produce the final spectrum from each sample. Standards used in the analysis were collected at the same beamline during previous beam runs. Beamline energy calibration was maintained by measurements of spectra from a stable reference (hydrogen uranyl phosphate) simultaneously with the collection of data from the experimental samples.

Analysis of the experimental spectra involved comparisons to standards. Then the data were numerically modelled to extract the structural parameters that describe the average atomic coordination around U. Valence state references included a sample of U^{VI} adsorbed to goethite, a nanoparticulate uraninite U^{IV} standard that was synthesized and characterized in previous work,[2] and a U^{IV}-carbonate complex. The U^{IV}-carbonate complex spectrum used to represent the complex in the LCF analysis was not obtained from a U^{IV}-carbonate reference compound, but from solid-phase U^{IV} produced by the reduction of U^{VI} by either bacteria or abiotically by 9,10-anthrahydroquinone-2,6-disulfonate (AH_2DS) in 30 mM bicarbonate media.[3] Normalization and background removal of the data were done using the program AUTOBK.[4] The numerical analysis of the spectra are based on the crystal structure of uraninite.[5] The code FEFF8[6] was used to generate the single-scattering contributions in the EXAFS for the O and U coordination shells in uraninite. Refinement of the numerical parameters against the experimental data was done in R-space using the program FEFFIT.[7]

As noted in the main text (Figure 4), there is significant similarity between the EXAFS data from the ChemGR 1h sample and a previously characterized U^{IV}-carbonate complex[3] and we followed the approach in our previous work to fit the data from the ChemGR 1h sample in the current study. We demonstrate that an EXAFS model consisting of an O and a U coordination shells is able to reproduce well the experimental data from a nanoparticulate uraninite standard (uraninite data are from Boyanov et al.,[3] the fit is shown in Figure S6-B and the resulting fit parameters are shown in Table S1-B). The EXAFS model for uraninite was then tested against the data from the ChemGR 1h sample (Figure S6-C and Table S1-C). The uraninite model does not reproduce well the outer-shell features in the spectrum, which indicates the predominance of other U^{IV} species in the ChemGR 1h sample. The presence of carbonate in the system suggests the possibility of U^{IV}-carbonate complexes. The structure and the EXAFS spectrum of a U^{IV}-carbonate crystal have been published[8]—it is a molecular crystal consisting of bi-dentate U^{IV}-carbonate complexes charge balanced by cations (Figure S7). The U^{IV}-carbonate complex is preserved in aqueous solution at pH 8.3 with bicarbonate excess.[8] Its EXAFS spectrum has been recreated in Figure S6-A from the fit parameters listed in that work. The characteristic features are the U-C contribution at 2.90 Å, as well as the overlapping contributions manifested in the peak around 3-4 Å resulting from the distal O atom in the carbonate group and the linear U-C-O multiple-scattering signals. We first attempted to fit the data from the ChemGR 1h sample with unconstrained C and O shells at distances appropriate for U^{IV}-carbonate complexation; however, the ΔR resolution of 0.19 Å(=π/2Δk) and the significant peak overlap over that distance resulted in fit parameter correlations and precluded unconstrained shell-by-shell fitting. Instead, the potential contribution from carbonate was included by numerically reproducing the signal from the U^{IV}-carbonate standard using the published fit values for the corresponding C and O_{dist} paths.[8] The amplitude of these standard-constrained C, O_{dist}, and C-O_{dist} multiple-scattering paths was weighed by a fraction variable x ($0<x<1$) in the model, and one ΔE variable was used to account for differences in the choice of edge energy between the previous work and here. This approach is similar to adding a spectral component in a linear combination fit. The overall fit with this model is shown in Figure S6-D (the contributions of the individual paths are illustrated in Figure S8). The addition of carbonate to the model resulted in a significant decrease of the χ_v^2 factor from 206 to 48 and in a significant improvement in the reproduction of the features missed by the nano-uraninite model. The obtained value of $x=0.52\pm0.1$ suggests that the spectral contribution of the carbonate ligands in the ChemGR 1h sample is about half of that in the well-ordered U^{IV}-carbonate standard. Overall, the fits suggest that a carbonate-complexed U^{IV} is the initial species resulting from reduction of U^{VI} by chemically-synthesized carbonate GR. It is possible that these U^{IV}-carbonate complexes occupy the interlayer space in the GR structure, are adsorbed as ternary =FeO-carbonate-U^{IV} complexes at edge sites of the Fe hydroxide layer, or are outer-sphere associated with the GR surface—these possibilities cannot be discerned by the EXAFS data. As shown in the main text, the initial U^{IV}-carbonate species evolve after a few days to form nanoparticulate uraninite.

The EXAFS data obtained from the BioGR system were best fit with a model consisting of an O, Fe, and O shell. The data were Fourier transformed at k^1, k^2, and k^3 weights ($FT[\chi(k)*k^n]$) and the three functions were fit simultaneously in R-space with the same fitting parameters. The purpose of multiple k-weight fitting is to provide additional contrast between light (e.g. O, C) and heavy (e.g. Fe) element contributions in the spectra, as the two generally have different amplitude dependencies with increasing k-values. By emphasizing the lower- or higher-k part of the spectrum using k^n-weighting, the relative proportion of light and heavy element contributions in the FT spectrum is changed (see orange and cyan lines in Figure S13), so if a heavy element contribution is fit with a light element shell there will be a misfit. The best fit for our data at all k-weights was obtained with a model consisting of an O, Fe, and O shell, as shown in Figure S13 and Table S3. The inclusion of the outer O shell in the EXAFS model was warranted because a fit without this shell resulted in a 5.7 fold increase of the reduced-χ^2 value of the fit (Table S3). It is possible that the signal fit by this shell is resulting from O atoms from farther binding sites on the surface of GR. However, fits of outer-shell EXAFS data are, in general, uncertain due to the potential contributions of multiple-scattering effects and/or an increased number of overlapping signals from several coordinating shells as the radial distance from the studied atom is increased. The data here do not allow differentiation between these signals, so we are modelling their aggregate contribution in the experimental spectrum as a single O shell with a resulting large coordination number and large disorder (i.e., Debye-Waller factor). The main purpose of the fit in Figure S13 is to determine the contribution of the closer Fe shell (at ~3 Å), the presence of which is interpreted as an indication of the U^{IV} adsorption complex at the GR surface. Thus, determining the exact origin of the signals modelled here by the 3rd coordination shell is not critical, but the presence of this signal in the fit is needed to produce a “background” or “overlap” contribution for the fit of the neighboring shells. As can be seen from Table S3, the fit parameters for the Fe shell are not significantly affected by the presence or absence of the outer O shell.

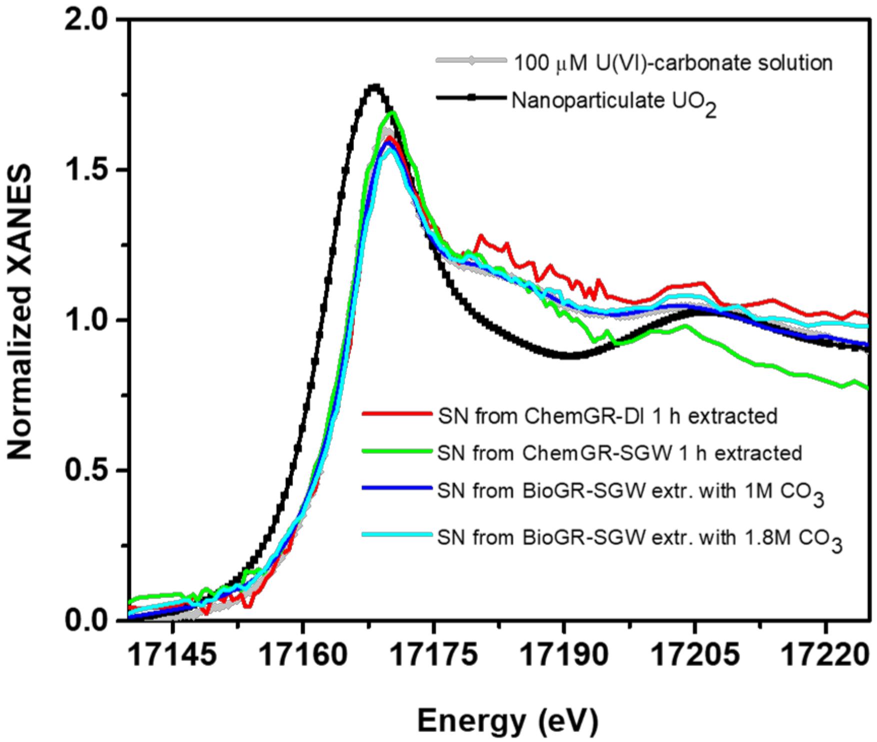

Figure S4. Comparisons of the XANES data from the carbonate extraction supernatants (SN) of the ChemGR and BioGR systems to the data from a 100 μM U^{VI}-carbonate solution standard and a nanoparticulate uraninite standard. The data overlay the U^{VI} standard, indicating that U^{VI} predominates in the extract solution.

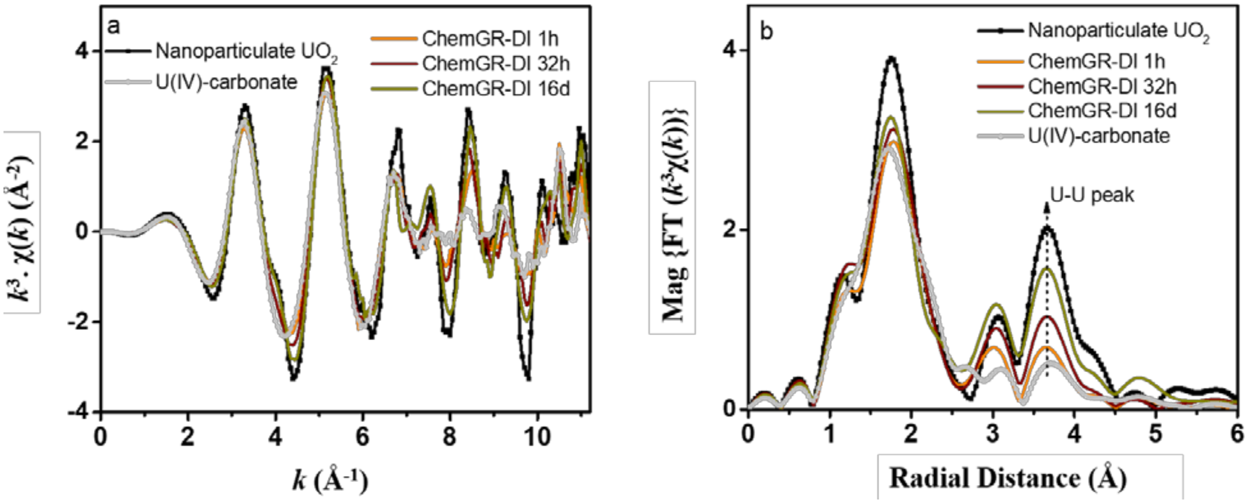

Figure S5. (a) k^{3}-weighted χ(k) EXAFS data and (b) Fourier transformed EXAFS data for ChemGR in DI-water system after 1 h, 32 h, and 16 d, plotted with nanoparticulate uraninite and U^{IV}-carbonate standards. The vertical dashed line indicates the peak in the FT EXAFS data resulting from the contribution of the U shell in uraninite. The Fourier transform is within the data range k = 2.2–10.4 Å^{-1} using 1.0-Å^{-1}-wide Hanning windowsills.

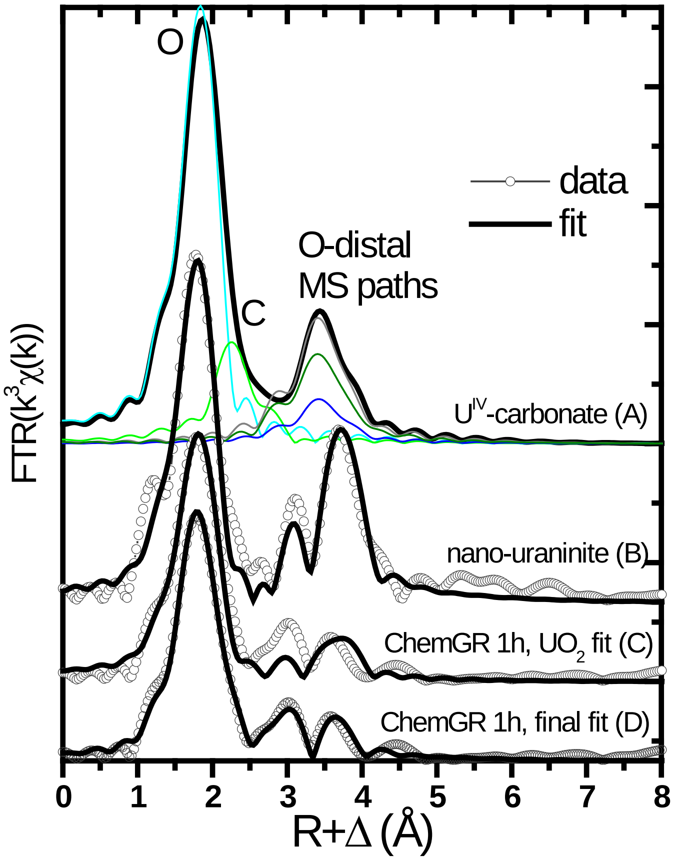

Figure S6. Fits of the U^{IV} EXAFS data from the ChemGR 1h sample: A) Reproduction of the fit to the experimental data from the U^{IV}-carbonate complex in Hennig et al.[8] The contribution of different paths are noted in color. B) fits of a nanoparticulate uraninite standard from Boyanov et al.[3] with the uraninite model described in the text; C) fit of the ChemGR 1h with the uraninite model; D) fit of the ChemGR 1h with carbonate groups added to the uraninite model. Data in symbols, fit is solid line. Fits are done over the range 1.4-4.0 Å. Numerical results are given in Table S1.

U-O2	2.40 Å
U-O14	2.41 Å
U-O5	2.42 Å
U-O10	2.42 Å
U-O7	2.43 Å
U-O11	2.49 Å
U-O4	2.50 Å
U-O8	2.51 Å
U-O1	2.52 Å
U-O13	2.52 Å
U-C3	2.90 Å
U-C2	2.90 Å
U-C1	2.91 Å
U-C4	2.92 Å
U-C5	2.92 Å
U-Na2	3.60 Å
U-Na3	3.88 Å
U-O6	4.16 Å
U-O9	4.16 Å
U-O12	4.16 Å
U-O3	4.17 Å
U-O15	4.18 Å
U-O2W	4.37 Å

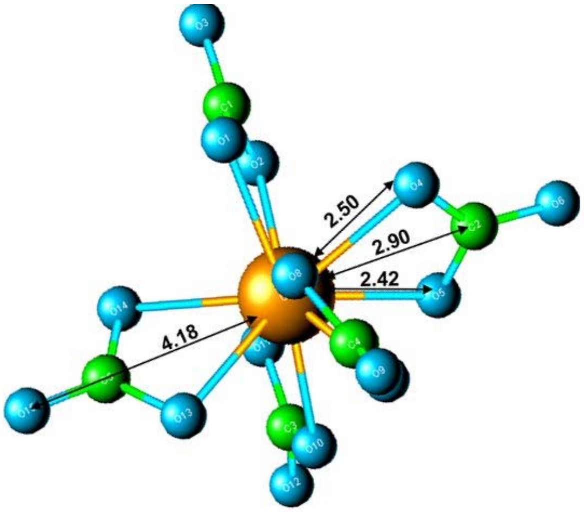

Figure S7. Structure of U^{IV}-carbonate, as determined in Hennig et al.[8] Some atoms are omitted for clarity. The carbonate groups are bidentate coordinated to the U^{IV} atom, with one short (~2.42 Å) and one long (~2.50 Å) U-O bond. Yellow atom: U^{IV}, blue atoms: O, green atoms: C atoms. The U, C, and distal O atoms form a nearly co-linear arrangement (U-C-O angle ~175 degree). The list on the left shows the distances of some of the coordinating atoms from the central U atom.

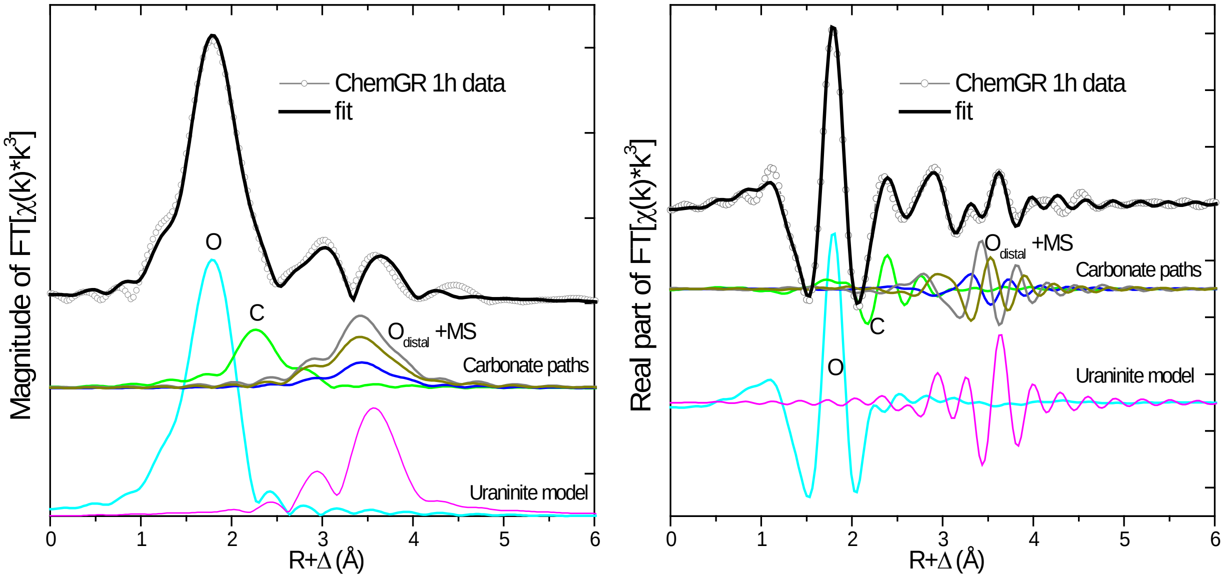

Figure S8. Details from the fits of the U^{IV} EXAFS data from the ChemGR 1h sample. Data are in symbols, fit is the solid line. The spectral contributions from the different atomic shells and multiple scattering contributions are presented in color. Fits are done over the range 1.4-4.0 Å. Numerical results are given in Table S1.

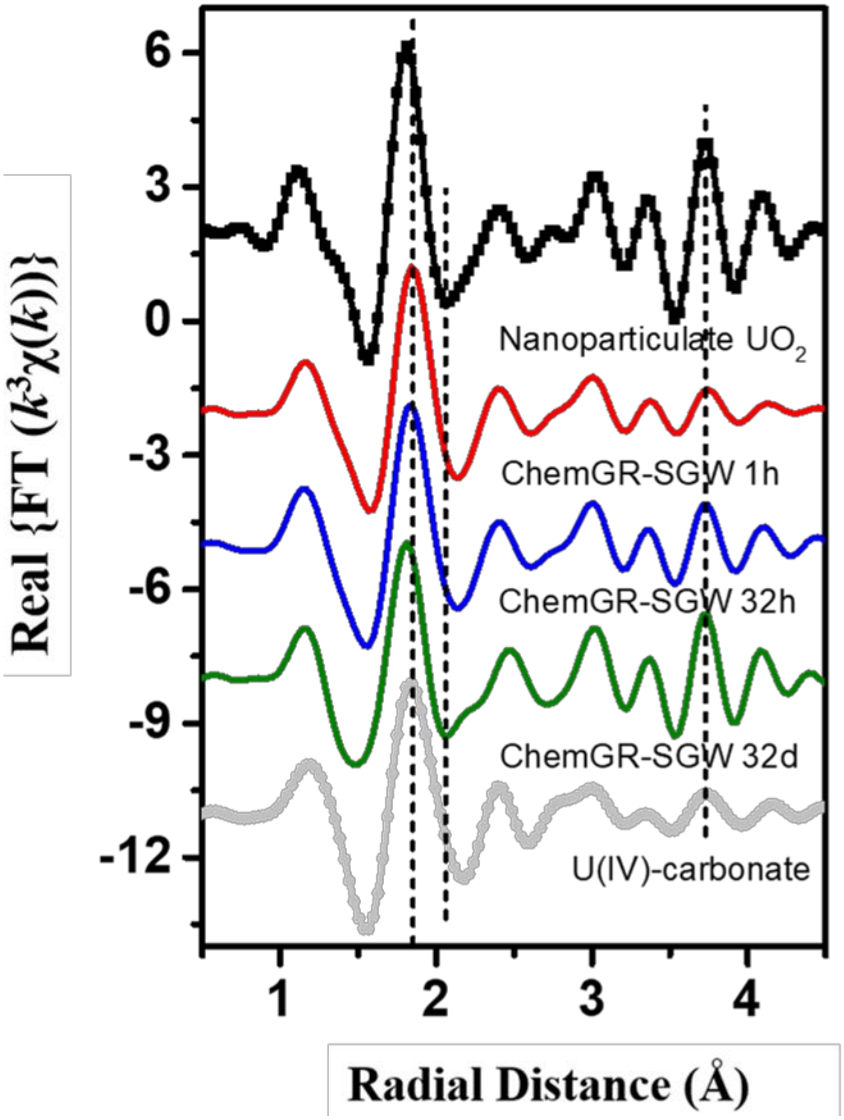

Figure S9. Real part of the Fourier transformed EXAFS data for ChemGR in the SGW system after 1 h, 32 h, and 32 d plotted with nanoparticulate uraninite and U^{IV}-carbonate standards. The vertical lines are guides to the eye for the positions of the different features. The lines at 1.8 Å and 2.1 Å correspond to the contribution of the O shell. The line at 3.7 Å corresponds to the contribution of the U shell in uraninite. The features at these positions show similarity of the 1-h sample to the U^{IV}-carbonate standard, whereas the 32-d sample is more similar to uraninite.

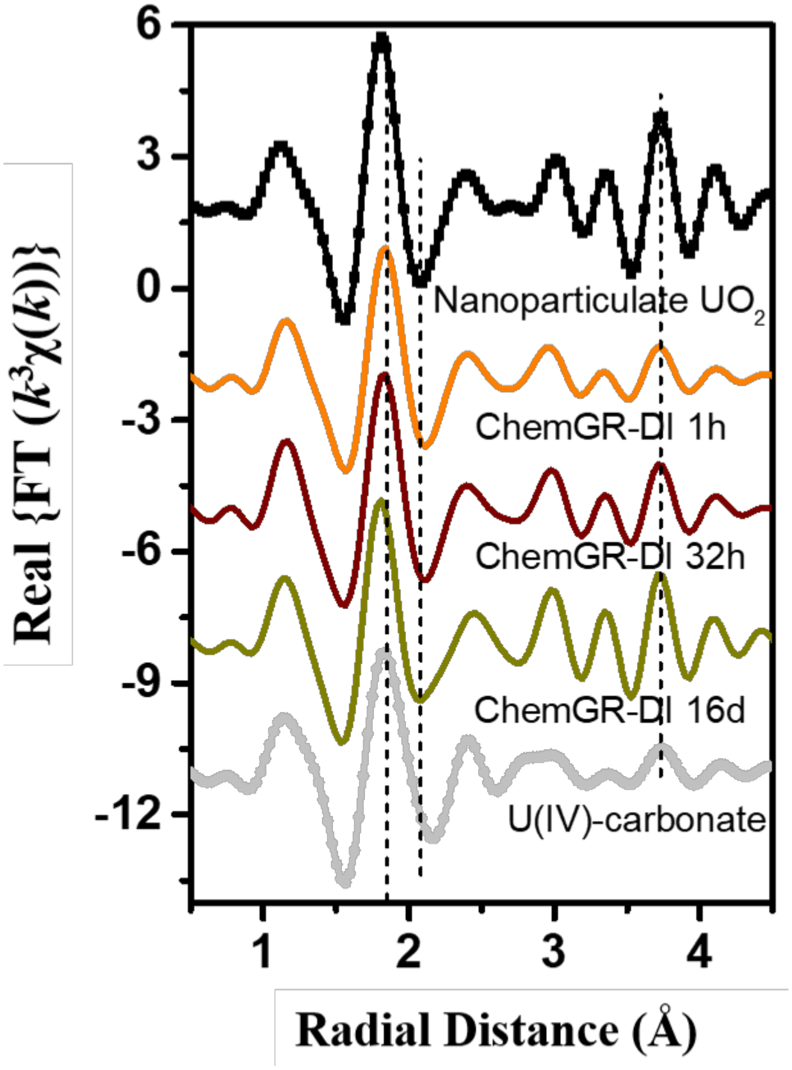

Figure S10. Real part of the Fourier transformed EXAFS data for the ChemGR system in the DI-water after 1 h, 32 h, and 16 d, plotted with nanoparticulate uraninite and U^{IV}-carbonate standards. The vertical lines are guides to the eye for the positions of the different features. The lines at 1.8 Å and 2.1 Å correspond to the contribution of the O shell, whereas the line at 3.7 Å corresponds to the contribution of the U shell in uraninite. The features at these positions show similarity of the 1-h sample to the U^{IV}-carbonate standard, whereas the 32-d sample is more similar to uraninite.

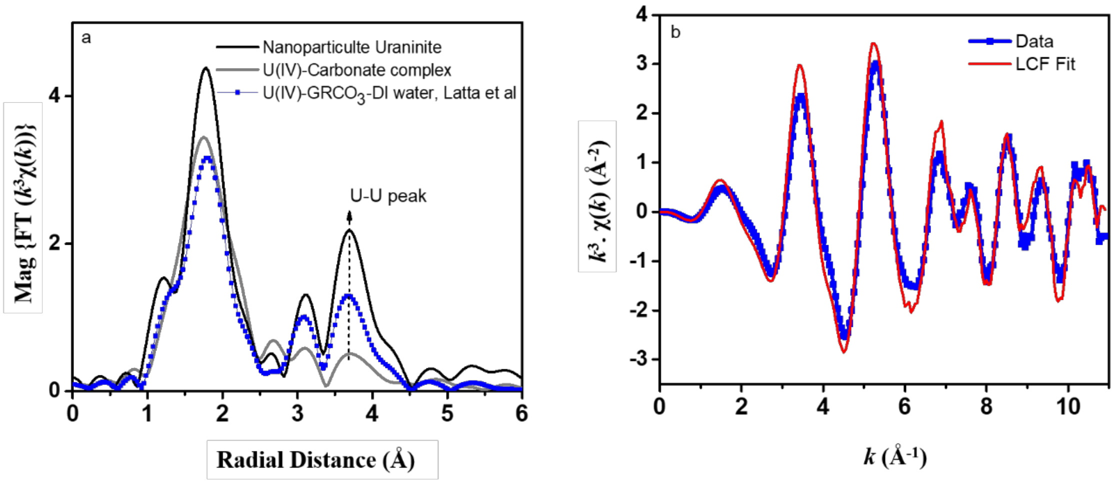

Figure S11. (a) Comparisons between the Fourier transformed EXAFS data from the 4-d ChemGR reactor with DI water in the study of Latta et al.[9] (symbols) to the nanoparticulate uraninite standard (black) and the carbonate-complexed U^{IV} spectrum (grey), both from Boyanov et al.[3] The Fourier transform is between k = 2.2–10.4 $Å^{-1}$. The vertical dashed line highlights the region where the U shell in uraninite contributes. Right: Linear combination fit between k = 2.2–10.4 $Å^{-1}$ of the $k^3\chi(k)$ data in Latta et al.[9] with the standards described above. The refined spectral proportions are 58% nanoparticulate uraninite and 42% carbonate-complexed U^{IV}.

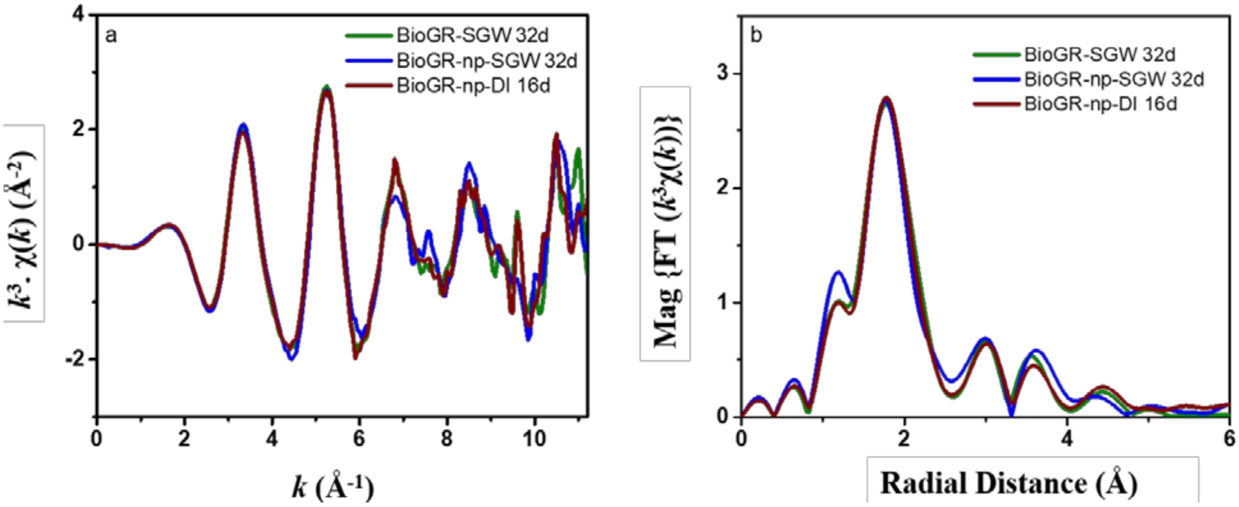

Figure S12. U L_{III} edge (a) k^3-weighted $\chi(k)$ EXAFS data and (b) Fourier-transformed EXAFS data for BioGR in the DI-water and SGW systems (np means the non-pasteurized samples).

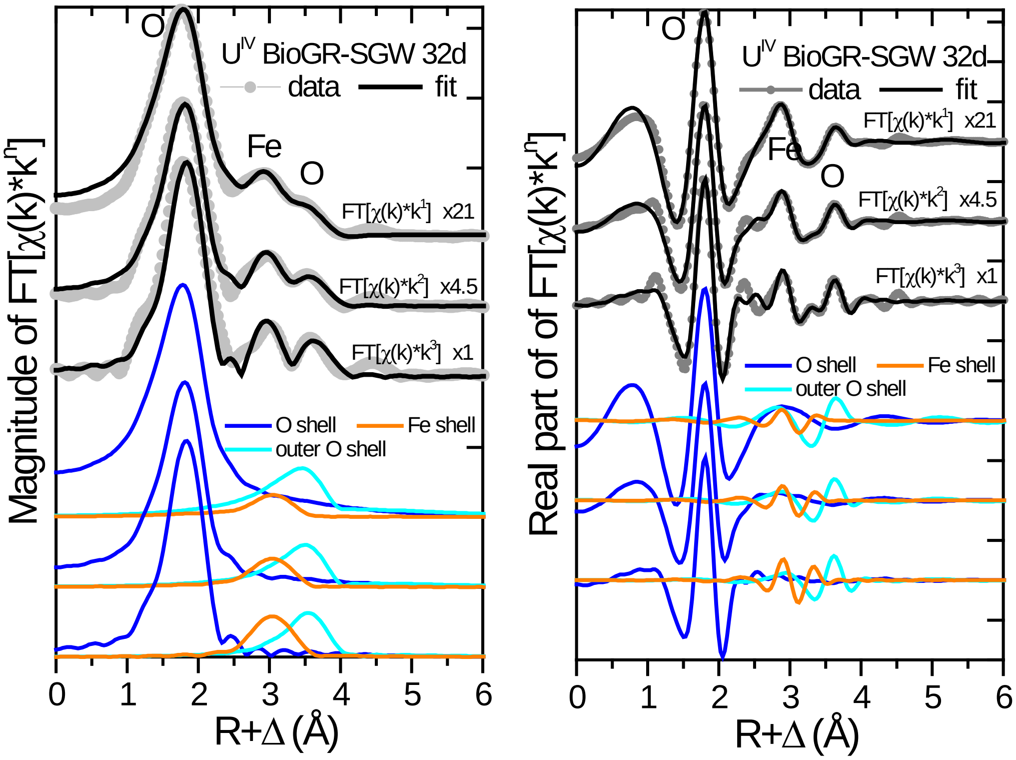

Figure S13. Best fit (line) of the BioGR EXAFS data (symbols) with a model consisting of an O, Fe, and O shell, as discussed in the text. The EXAFS data from the BioGR sample are Fourier transformed at k^1, k^2, and k^3 weight (FT[χ(k)*k^n]) and the three functions are fit simultaneously in R-space with the same fitting parameters shown in Table S2. The scaling factors shown to the right of each graph are applied to both data and fit for better presentation of the three sets on the same graph. The scaled individual contributions of each shell are illustrated below in colored lines for the corresponding k-weight of the FT (note that the individual contributions combine linearly only in the real part of the FT to produce the fit line, not in the magnitude). The Fourier transforms are between k= 2.2 – 10.4 Å^{-1}, fits are between R+Δ = 1.5 – 4.0 Å.

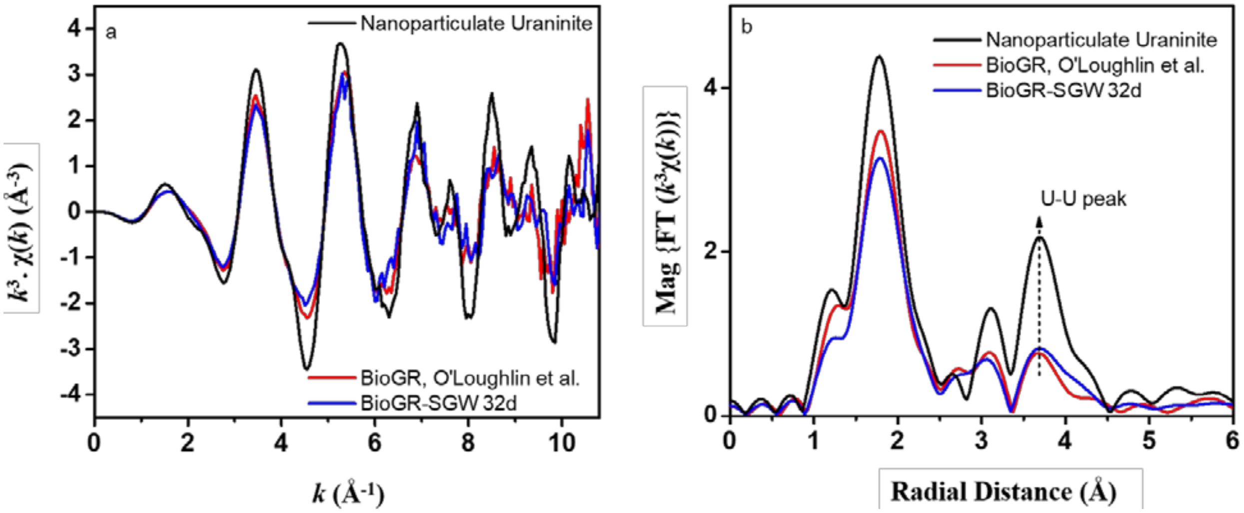

Figure S14. Comparisons between the BioGR data in this study (blue) to that in the carbonate BioGR reactor of O'Loughlin et al.[10] (red), showing the same EXAFS data within measurement uncertainty. The data are compared to the nanoparticulate uraninite standard (black). Left: $k^3\chi(k)$ data. Right: Fourier transform between k = 2.2– 0.4 Å^{-1} using 1.0 Å^{-1} Hanning windowsills.

Table S1. Numerical results from modeling of the EXAFS data from the uraninite standard and the ChemGR 1h sample.

Path	N	R(Å)	σ^2 (Å^2)	ΔE(eV)	DF	R-factor	χ_ν^2
A) U(IV)-carbonate model recreated from Hennig et al. (2010)							
U-O	10.2	2.45	0.0092	-2.1			
U-C	4.3	2.91	0.0044				
U-Odist	5.1	4.17	0.0057				
U-C-Odist	2x5.1	4.17	0.0057				
U-C-Odist-C	5.1	4.17	0.0057				
B) nano-uraninite data, single-scattering uraninite model[a]							
U-O	8.0 ± 1.3	2.34 ± 0.01	0.0129 ± 0.0023	0.4 ± 1.6	7	0.029	188
U-U	5.2 ± 2.1	3.84 ± 0.02	0.0065 ± 0.0030	0.9 ± 2.2			
C) data from 1h ChemGR sample, single-scattering uraninite model							
U-O	6.4 ± 1.1	2.35 ± 0.02	0.0140 ± 0.0028	1.5 ± 1.8	8	0.054	206
U-U	1.3 ± 0.6	3.77 ± 0.06	0.0065[b]	1.3 ± 7.0			
D) data from 1h ChemGR sample, uraninite + weighed U(IV)-carbonate model							
U-O	5.2 ± 0.6	2.33 ± 0.01	0.0116 ± 0.0015	-0.8 ± 1.1	6	0.009	48
U-U	2.8 ± 0.4	3.74 ± 0.01	0.0065[b]	-4.4 ± 2.1			
x[c]	0.52 ± 0.10			1.9 ± 1.1			

When uncertainties are not given for a parameter, the parameter is fixed to the indicated value. DF=Degrees of Freedom in the fit. The R-factor is a normalized sum of the squared differences between model and fit. χ_ν^2 is a goodness-of-fit parameter accounting for the amount of data and number of variables in the fit. More information for these parameters can be found in the FEFFIT manual.

[a] In the “single-scattering uraninite” model fits, the data from nanoparticulate uraninite was modeled with free O and U shells. In all other fits, the U shell Debye-Waller factor was fixed to that in nanoparticulate uraninite and the coordination number was refined.
[b] Parameter held fixed to that refined in nanoparticulate uraninite
[c] Fraction variable *x* ($0<x<1$) by which the amplitudes of the U-C, U-Odist, and multiple-scattering paths in model (A) were multiplied when added in model (C)

Table S2. The relative fraction of U^{IV} species as calculated by linear combination fitting of the k^2 weighted χ(k) data using nanoparticulate uraninite and U^{IV}-carbonate standards

Sample ID/U^{IV} Species	U^{IV}-Carbonate	Uraninite
ChemGR in SGW		
ChemGR-SGW 1 h	92%	8%
ChemGR-SGW 32 h	75%	25%
ChemGR-SGW 32 d	23%	77%
ChemGR in DI-water		
ChemGR-DI 1 h	76%	24%
ChemGR-DI 32 h	67%	33%
ChemGR-DI 16 d	25%	75%

Table S3. The best fit values for EXAFS modeling of a representative BioGR sample

Path	CN	Distance (Å)	σ^2 (Å^2)*10^{-3}	E_0(eV)	DF	χ_v^2	R-factor
Fit with the outer O shell					5.5	234	0.016
O	5.2 ± 0.4	2.35 ± 0.01	12.1 ± 1.9	-1.5 ±0.7			
Fe	2.0 ± 0.7	3.49 ± 0.02	15.0#	-1.5 ±0.7			
O	10.0 ± 3.3	4.16 ± 0.02	16.7 ± 7.9	-1.5 ±0.7			
Fit without the outer O shell					8.5	1335	0.072
O	5.2 ± 1.1	2.37 ± 0.02	12.4 ± 4.4	-0.4 ±1.7			
Fe	2.7 ± 1.5	3.54 ± 0.05	15.0#	-0.4 ±1.7			

#The σ^2 value of the Fe shell was constrained to the same value as in Latta et al.[9] to minimize large correlations between σ^2 and coordination number for this shell and to allow comparisons between the two studies. DF=degrees of freedom in the fit; χ_v^2 is the reduced chi-square of the fit; R-factor is the fractional misfit relative to the amplitude of the data. More details on these fit indicators can be found in the FEFFIT documentation.

REFERENCES:

(1) Segre, C. U.; Leyarovska, N. E.; Chapman, L. D.; Lavender, W. M.; Plag, P. W.; King, A. S.; Kropf, A. J.; Bunker, B. A.; Kemner, K. M.; Dutta, P.; Duran, R. S.; Kaduk, J. *The MRCAT insertion device beamline at the Advanced Photon Source*, In: Pianetta, P., Arthur, J., Brennan, S., Ed. 11th US National Conference on Synchrotron Radiation Instrumentation. American Institute of Physics, New York, pp 419-422.

(2) Latta, D. E.; Kemner, K. M.; Mishra, B.; Boyanov, M. I. Effects of calcium and phosphate on uranium(IV) oxidation: Comparison between nanoparticulate uraninite and amorphous U^{IV}-phosphate. *Geochim. Cosmochim. Acta* **2016,** *174*, 122-142.

(3) Boyanov, M. I.; Fletcher, K. E.; Kwon, M. J.; Rui, X.; O'Loughlin, E. J.; Loffler, F. E.; Kemner, K. M. Solution and microbial controls on the formation of reduced U(IV) species. *Environ. Sci. Technol.* **2011,** *45* (19), 8336-8344.

(4) Newville, M.; Livins, P.; Yacoby, Y.; Rehr, J. J.; Stern, E. A. Near-edge X-ray-absorption fine-structure of Pb: A comparison of theory and experiment. *Phys. Rev. B* **1993,** *47* (21), 14126-14131.

(5) Wyckoff, R. W. G., *Crystal Structures*. 2 ed.; John Wiley & Sons: New York, 1964.

(6) Ankudinov, A. L.; Ravel, B.; Rehr, J. J.; Conradson, S. D. Real-space multiple-scattering calculation and interpretation of X-ray-absorption near-edge structure. *Phys. Rev. B* **1998,** *58* (12), 7565-7576.

(7) Newville, M.; Ravel, B.; Haskel, D.; Rehr, J. J.; Stern, E. A.; Yacoby, Y. Analysis of multiple-scattering XAFS data using theoretical standards. *Physica B* **1995,** *208* (1-4), 154-156.

(8) Hennig, C.; Ikeda-Ohno, A.; Emmerling, F.; Kraus, W.; Bernhard, G. Comparative investigation of the solution species $[U(CO_3)_5]^{6-}$ and the crystal structure of $Na_6[U(CO_3)_5]\cdot 12H_2O$. *Dalton T.* **2010,** *39* (15), 3744-3750.

(9) Latta, D. E.; Boyanov, M. I.; Kemner, K. M.; O'Loughlin, E. J.; Scherer, M. Reaction of uranium(VI) with green rusts: Effect of interlayer anion. *Curr. Inorg. Chem.* **2015,** *5* (3), 156-168.

(10) O'Loughlin, E. J.; Kelly, S. D.; Kemner, K. M. XAFS investigation of the interactions of U(VI) with secondary mineralization products from the bioreduction of Fe(III) oxides. *Environ. Sci. Technol.* **2010,** *44* (5), 1656-1661.